BornAgain

Incomplete Physics Manual

Software version 1.16

This document last updated March 27, 2020

Gennady Pospelov, Walter Van Herck, Joachim Wuttke

Scientific Computing Group
Jülich Centre for Neutron Science
at Heinz Maier-Leibnitz Zentrum Garching
Forschungszentrum Jülich GmbH

Contents

Preface

About BornAgain

BornAgain is a software package to simulate and fit reflectometry, off-specular scattering, and grazing-incidence small-angle scattering (GISAS) of X-rays and neutrons. It provides a generic framework for modeling multilayer samples with smooth or rough interfaces and with various types of embedded nanoparticles. The name, BornAgain, alludes to the central role of the distorted-wave Born approximation (DWBA) in the physical description of the scattering process.

BornAgain is maintained by the Scientific Computing Group of the Jülich Centre for Neutron Science (JCNS) at Heinz Maier-Leibnitz Zentrum (MLZ) Garching, Germany. It free and open source software. The source code is released under the GNU General Public License (GPL, version 3 or higher), the documentation under the Creative Commons license CC-BY-SA.

This manual vs other documentation

This Physics Manual explains some of the theory behind BornAgain. It is restricted to topics that are not covered by other components of the BornAgain documentation. These include:

- Our 2020 article in J. Appl. Cryst. [1] that gives a broad overview over BornAgain. The implemented physics is summarized in Sect. 5.

- The web site `https://www.bornagainproject.org`, which includes instructions how to download and install BornAgain, and extensive tutorials on setting up physical models.

- The complete documentation of the Application Programming Interface (API), which can be generated by running the open-source tool *Doxygen* over the source code.

- Further technical documents, available from the *Documents* tab on the download page. So far, there exists one such document, namely the Form factor catalog.

This Physics Manual is work in progress. In future editions, it may grow as we elaborate details or add new chapters, but it may also shrink as we move contents to journal articles or other documents.

Citation

The canonical reference for BornAgain is the journal article [1]

> Gennady Pospelov, Walter Van Herck, Jan Burle, Juan M. Carmona Loaiza, Céline Durniak, Jonathan M. Fisher, Marina Ganeva, Dmitry Yurov and Joachim Wuttke:
> BornAgain: software for simulating and fitting grazing-incidence small-angle scattering
> J. Appl. Cryst. 53, 262–276 (2020)

Use of the software should additionally be documented by citing a specific version thereof:

> BornAgain — Software for simulating and fitting X-ray and neutron small-angle scattering at grazing incidence, version ⟨`version`⟩ (⟨`release date`⟩),
> http://www.bornagainproject.org

Citation of the present Physics Manual is only necessary when referring to specific information. As this document is subject to frequent and substantial change, it is important to refer to a specific edition by indicating the release date printed on the title page:

> Gennady Pospelov, Walter Van Herck, Joachim Wuttke:
> BornAgain Physics Manual (⟨`release date`⟩),
> http://www.bornagainproject.org

Old editions can be retrieved from the BornAgain source repository.

The initial design of BornAgain and much of the implemented physics owe much to the widely used program IsGISAXS by Rémi Lazzari [2]. Depending on how BornAgain is used in scientific work, it may be appropriate to cite the pioneering papers by Lazzari *et al.* [3, 4].

Typographic Conventions

We use the following colored boxes to highlight certain information:

> Such a box contains a **warning** about potential problems with the software or the documentation.

> This road sign in the margin indicates **work in progress**.

> An **implementation note** explains how the theory exposed in this manual is actually used in BornAgain.

> This is a link.

Mathematical notations are explained in the symbol index, page 48.

This document is formatted for single-sided printing, which is more convenient for reading on a screen.

1 Scattering

This chapter provides a self-contained introduction into the theory of neutron and X-ray scattering, as needed for the analysis of grazing-incidence small-angle scattering (GISAS) experiments. In Section 1.1, a generic wave equation is derived. In Section 1.2, it is solved in first-order distorted-wave Born approximation (DWBA). The chapter finishes with a qualitative discussion of coherence lengths in Section 1.3.

1.1 Wave propagation

In this section, we review the wave equations that describe the propagation of neutrons (Secs. 1.1.1 and 1.1.2) and X-rays (Sec. 1.1.3) in matter, and combine them into a unified wave equation (Sec. 1.1.4) that is the base for the all following analysis. This provides justification and background for Eqns. 1–3 in the BornAgain reference paper [1].

1.1.1 Neutrons in a scalar potential

The scalar wavefunction $\psi(\boldsymbol{r}, t)$ of a free neutron in absence of a magnetic field is governed by the Schrödinger equation

$$i\hbar\partial_t \psi(\boldsymbol{r}, t) = \left[-\frac{\hbar^2}{2m}\boldsymbol{\nabla}^2 + V(\boldsymbol{r}) \right] \psi(\boldsymbol{r}, t). \tag{1.1}$$

Since BornAgain only aims at modelling elastic scattering, any time dependence of the potential is averaged out in the definition $V(\boldsymbol{r}) \coloneqq \langle V(\boldsymbol{r}, t) \rangle$. Inelastic scattering, in principle, can be accounted for by an extra contribution damping.[1] Therefore we only need to consider monochromatic waves with given frequency ω. In consequence, the wavefunction

$$\psi(\boldsymbol{r}, t) = \psi(\boldsymbol{r})\mathrm{e}^{-i\omega t} \tag{1.2}$$

factorizes into a stationary wave and a time-dependent phase factor. In the following, we will characterize the incoming radiation not by its energy $\hbar\omega$, but by its *vacuum wavenumber* K, given by the dispersion relation

$$\hbar\omega = \frac{(\hbar K)^2}{2m}. \tag{1.3}$$

---

[1] This is not explicitly supported in the software, but users are free to increase the imaginary part of the refractive index to emulate damping by inelastic losses.

We shall use Fermi's pseudopotential in the rescaled form[2]

$$v(\boldsymbol{r}) := \frac{2m}{\hbar^2} V(\boldsymbol{r}) = 4\pi \sum_j \langle b_j \delta\left(\boldsymbol{r} - \boldsymbol{r}_j(t)\right)\rangle. \tag{1.4}$$

The Schrödinger equation (1.1) then takes the simple form

$$\left[\boldsymbol{\nabla}^2 + K^2 - v(\boldsymbol{r})\right] \psi(\boldsymbol{r}) = 0. \tag{1.5}$$

The sum runs over all nuclei exposed to ψ. The *bound scattering length* b_j is isotope specific; values are tabulated [5].

In small-angle scattering, as elsewhere in neutron optics [6], the potential can be coarse-grained by spatially averaging over at least a few atomic diameters,

$$v(\boldsymbol{r}) = \sum_s b_s \rho_s(\boldsymbol{r}), \tag{1.6}$$

where the sum now runs over chemical elements, $b_s := \langle b_j \rangle_{j \in s}$ is the bound *coherent scattering length*, and ρ_s is a number density. In passing from (1.4) to (1.6), we neglected Bragg scattering from atomic-scale correlation, and incoherent scattering from spin or isotope related fluctuations of b_j. In small-angle experiments, these types of scattering only matter as loss channels.[3] Furthermore, incoherent scattering, as inelastic scattering, contributes to the diffuse background in the detector. In conclusion, the coarse-grained neutron optical potential (1.6) is just a *scattering length density* (SLD) [6, eq. 2.8.37].

1.1.2 Neutrons in a magnetic field

In presence of a magnetic field, the propagation of free neutrons becomes spin dependent. Therefore the scalar wavefunction of Sec. 1.1.1 must be replaced by spinor $\boldsymbol{\Psi}$. The magnetic moment μ of the neutron couples to the magnetic induction $\boldsymbol{B}$ [7, 8]. With the coupling term, the Schrödinger equation (1.1) becomes

$$\left[-\frac{\hbar^2}{2m}\boldsymbol{\nabla}^2 + V(\boldsymbol{r}) + \mu\boldsymbol{B}(\boldsymbol{r})\hat{\boldsymbol{\sigma}} - \hbar\omega\right] \boldsymbol{\Psi}(\boldsymbol{r}) = 0, \tag{1.7}$$

where μ_0 is the vacuum permeability, and $\hat{\boldsymbol{\sigma}}$ is the Pauli vector, composed of the three Pauli matrices. We introduce the reduced field

$$\boldsymbol{b} := \frac{2m\mu_0\mu_{\mathrm{n}}}{\hbar^2}\boldsymbol{B}, \tag{1.8}$$

to rewrite the Schrödinger equation in analogy to (1.5) as

$$\left[\boldsymbol{\nabla}^2 + K^2 - v(\boldsymbol{r}) - \boldsymbol{b}(\boldsymbol{r})\hat{\boldsymbol{\sigma}}\right] \boldsymbol{\Psi}(\boldsymbol{r}) = 0. \tag{1.9}$$

---

[2]From here on, our notation differs by a factor of 4π from that in our 2020 paper [1].

[3]Same remark as in Footnote 1: To model these losses, use the imaginary part of the refractive index.

1.1.3 X-rays

The propagation of X-rays is governed by Maxwell's equations, which read in SI units

$$\boldsymbol{\nabla} \times \boldsymbol{E} = -\partial_t \boldsymbol{B}, \quad \boldsymbol{\nabla} \boldsymbol{B} = 0, \quad \boldsymbol{B} = \boldsymbol{\mu}(\boldsymbol{r})\mu_0 \boldsymbol{H},$$

$$\boldsymbol{\nabla} \times \boldsymbol{H} = +\partial_t \boldsymbol{D}, \quad \boldsymbol{\nabla} \boldsymbol{D} = 0, \quad \boldsymbol{D} = \boldsymbol{\epsilon}(\boldsymbol{r})\epsilon_0 \boldsymbol{E}. \tag{1.10}$$

Since BornAgain only addresses elastic scattering, we assume the permeability and permittivity tensors $\boldsymbol{\mu}$ and $\boldsymbol{\epsilon}$ to be time-independent. Therefore, as in Sec. 1.1.1, we only need to consider monochromatic waves with given frequency ω, and each of the fields $\boldsymbol{E}$, $\boldsymbol{D}$, $\boldsymbol{H}$, $\boldsymbol{B}$ factorizes into a stationary field and a time-dependent phase factor.[4] We will formulate the following in terms of the electric field

$$\boldsymbol{E}(\boldsymbol{r}, t) = \boldsymbol{E}(\boldsymbol{r}) e^{-i\omega t}. \tag{1.11}$$

The other three fields can be obtained from $\boldsymbol{E}$ by straightforward application of (1.10).

Since magnetic refraction or scattering is beyond the scope of BornAgain, the relative magnetic permeability tensor is always $\boldsymbol{\mu}(\boldsymbol{r}) = 1$. As customary in SAXS and GISAXS, we assume that the dielectric properties of the material are those of a polarizable electron cloud.[5] Thereby the relative dielectric permittivity tensor $\boldsymbol{\epsilon}$ becomes a scalar,

$$\epsilon(\boldsymbol{r}) = 1 - \frac{4\pi r_e}{K^2} \rho(\boldsymbol{r}), \tag{1.12}$$

with the classical electron radius $r_e = e^2/(4\pi\epsilon_0 m c^2) \simeq 2.8 \cdot 10^{-15}$ m, the electron number density $\rho(\boldsymbol{r})$, and the vacuum wavenumber K, given by the dispersion relation

$$K^2 = \mu_0 \epsilon_0 \omega^2 = \omega^2/c^2. \tag{1.13}$$

With these simplifying assumptions about $\boldsymbol{\epsilon}$ and $\boldsymbol{\mu}$, Maxwell's equations yield the wave equation

$$\boldsymbol{\nabla} \times \boldsymbol{\nabla} \times \boldsymbol{E} = K^2 \epsilon(\boldsymbol{r}) \boldsymbol{E}. \tag{1.14}$$

Using a standard identity from vector analysis, it can be brought into the more tractable form

$$\left[\boldsymbol{\nabla}^2 - \boldsymbol{\nabla} \cdot \boldsymbol{\nabla} + K^2 \epsilon(\boldsymbol{r}) \right] \boldsymbol{E}(\boldsymbol{r}) = 0. \tag{1.15}$$

---

[4]This phase factor can be defined with a plus or a minus sign in the exponent. Most texts on X-ray crystallography, including influential texts on GISAXS [4], prefer the *crystallographic convention* with a plus sign. In BornAgain, we prefer the opposite *quantum-mechanical convention* for consistency with the neutron case (1.2), where the minus sign is an inevitable consequence of the standard form of the Schrödinger equation.

[5]This is occasionally called the *Laue model* [9].

1.1.4 Unified wave equation

We combine all the above in a unified wave equation

$$[\boldsymbol{D}_0 - \boldsymbol{V}(\boldsymbol{r})]\,\boldsymbol{\Psi}(\boldsymbol{r}) = 0 \tag{1.16}$$

with the vacuum wave operator

$$\boldsymbol{D}_0 := \begin{cases} \boldsymbol{\nabla}^2 + K^2 & \text{for neutrons,} \\ \boldsymbol{\nabla}^2 - \boldsymbol{\nabla}\cdot\boldsymbol{\nabla} + K^2 & \text{for X-rays} \end{cases} \tag{1.17}$$

and the potential

$$\boldsymbol{V}(\boldsymbol{r}) := \begin{cases} v(\boldsymbol{r}) & \text{for neutrons (scalar),} \\ v(\boldsymbol{r}) + \boldsymbol{b}(\boldsymbol{r})\hat{\boldsymbol{\sigma}} & \text{for neutrons (spinorial),} \\ K^2(\epsilon(\boldsymbol{r}) - 1) & \text{for X-rays.} \end{cases} \tag{1.18}$$

The generic wave amplitude $\boldsymbol{\Psi}$ shall represent the scalar neutron wavefunction ψ, the spinor $\boldsymbol{\Psi}$, or the electric vector field $\boldsymbol{E}$, as applicable.

1.1.5 Density operator, flux

An eigenfunction of the vacuum wave operator $\boldsymbol{D}_0$ is a plane wave with real wavevector $\boldsymbol{k}$. In the spinor or vector case, its polarization shall be expressed in an orthonormal base $\{\boldsymbol{u}_\alpha\}$ with $\alpha = 1, 2$ (for spin $1/2$ or for traverse electric field in vacuum). The corresponding eigenstate can be written as ket $|\boldsymbol{k}\alpha\rangle$, the real-space coordinate representation as

$$\boldsymbol{\Psi}_{\boldsymbol{k}\alpha}(\boldsymbol{r}) \equiv \langle\boldsymbol{r}|\boldsymbol{k}\alpha\rangle = (2\pi)^{-3/2}\boldsymbol{u}_\alpha \mathrm{e}^{i\boldsymbol{k}\boldsymbol{r}}. \tag{1.19}$$

The incident neutron beam in an actual scattering experiment is not such a *pure* state, but a statistical mixture of states, and must therefore be described by the density operator

$$\boldsymbol{\rho} := \sum_{\boldsymbol{k}\alpha} p_{\boldsymbol{k}\alpha}\,|\boldsymbol{k}\alpha\rangle\,\langle\boldsymbol{k}\alpha|\,, \tag{1.20}$$

where $p_{\boldsymbol{k}\alpha}$ quantifies the contribution of pure state $|\boldsymbol{k}\alpha\rangle$.

In quantum mechanics, the current density, or flux, is measured by the operator

$$\boldsymbol{J} := \frac{1}{2}\big[\,|\boldsymbol{r}\rangle\,\langle\boldsymbol{r}|\,\boldsymbol{k} + \boldsymbol{k}\,|\boldsymbol{r}\rangle\,\langle\boldsymbol{r}|\,\big]. \tag{1.21}$$

With (1.20), we obtain

$$\boldsymbol{J}(\boldsymbol{r}) := \mathrm{Tr}(\boldsymbol{\rho}\boldsymbol{J}) = \sum_{\boldsymbol{k}\alpha} p_{\boldsymbol{k}\alpha}\,\mathrm{Re}(\boldsymbol{k})\,|\boldsymbol{\Psi}_{\boldsymbol{k}\alpha}|^2. \tag{1.22}$$

In the electromagnetic case, the energy flux is given by the Poynting vector, which for complex fields takes the form

$$\boldsymbol{S} := \mathrm{Re}(\boldsymbol{E}(\boldsymbol{r}, t)) \times \mathrm{Re}(\boldsymbol{H}(\boldsymbol{r}, t)). \tag{1.23}$$

For a stationary plane wave $\boldsymbol{E}(\boldsymbol{r}) = \boldsymbol{E_k}\mathrm{e}^{i\boldsymbol{kr}}$ in vacuum, we find

$$S = \frac{1}{2\omega\mu_0}|\boldsymbol{E_k}|^2 \,\mathrm{Re}\,\boldsymbol{k}, \tag{1.24}$$

which confirms the common knowledge that the radiation intensity counted in a detector is proportional to the squared electric field amplitude. At constant frequency, the prefactor is ignorable so that we can use the quantum-mechanical flux (1.22) also for x-rays.

1.2 Distorted-wave Born approximation

To describe scattering from a condensed-matter sample, the wave equation is solved through a perturbation expansion. The ordinary form of this expansion, the *Born approximation* (BA), is derived in many textbooks.[6] For scattering under grazing-incidence, however, the more generic *distorted-wave Born approximation* (DWBA)[7] is required. In this section, we provide a self-contained derivation based on the unified neutron and X-ray wave equation (1.16).

1.2.1 Distortion versus perturbation

To get started, we decompose the potential (1.18) into a more regular and a more fluctuating part:

$$\boldsymbol{V}(\boldsymbol{r}) =: \boldsymbol{\Lambda}(\boldsymbol{r}) + \boldsymbol{U}(\boldsymbol{r}). \tag{1.25}$$

The *distortion field* $\boldsymbol{\Lambda}$ comprises regular, well-known features of the sample. The *perturbation potential* $\boldsymbol{U}$ stands for the more irregular, unknown features of the sample one ultimately wants to study in a scattering experiment. This is vague, and in certain situations the decomposition (1.25) is indeed to some extent arbitrary. However, in most practical cases $\boldsymbol{\Lambda}$ and $\boldsymbol{U}$ are clearly determined by the following basic idea of DWBA:

---

[6]For a particularly detailed derivation see Schober's lecture notes on neutron scattering [10].

[7]The DWBA was originally devised by Massey and Mott (ca 1933) for collisions of charged particles. Summaries can be found in some quantum mechanics textbooks (Messiah, Schiff) and in monographs on scattering theory (e. g. Newton). The first explicit applications to grazing-incidence scattering were published in 1982: Vineyard [11] discussed X-ray scattering, but failed to account for the distortion of the scattered wave; Mazur and Mills [12] deployed heavy formalism to compute the inelastic neutron scattering cross section of ferromagnetic surface spin waves from scratch. A concise derivation of the DWBA cross section was provided by Dietrich and Wagner (1984/85) for X-rays [13] and neutrons [14]. Unfortunately, their work was overlooked in much of the later literature, which often fell back to less convincing derivations.

The wave equation (1.16) shall henceforth be written as

$$\boldsymbol{D}(\boldsymbol{r})\boldsymbol{\Psi}(\boldsymbol{r}) = \boldsymbol{U}(\boldsymbol{r})\boldsymbol{\Psi}(\boldsymbol{r}) \tag{1.26}$$

with the *distorted wave operator*

$$\boldsymbol{D}(\boldsymbol{r}) \coloneqq \boldsymbol{D}_0 - \boldsymbol{\Lambda}(\boldsymbol{r}). \tag{1.27}$$

Only $\boldsymbol{U}$ shall be treated as a perturbation. The propagation of incident and scattered waves under the influence of $\boldsymbol{\Lambda}$, in contrast, shall be handled exactly, through analytical solution of the unperturbed distorted wave equation

$$\boldsymbol{D}(\boldsymbol{r})\boldsymbol{\Psi}(\boldsymbol{r}) = 0. \tag{1.28}$$

The solutions are called *distorted* because they differ from the *plane* waves obtained in the vacuum case $\boldsymbol{\Lambda} = 0$.

Except for neutrons in a magnetic field the distortion field is scalar so that it can be expressed through the *refractive index*

$$n(\boldsymbol{r}) \coloneqq \sqrt{1 - \frac{4\pi\Lambda(\boldsymbol{r})}{K^2}} = \begin{cases} \sqrt{1 - 4\pi\overline{v}(\boldsymbol{r})/K^2} & \text{for neutrons,} \\ \sqrt{\epsilon(\boldsymbol{r})} & \text{for X-rays.} \end{cases} \tag{1.29}$$

If $\overline{v}(\boldsymbol{r})$ or $\epsilon(\boldsymbol{r})$ has an imaginary part, describing absorption, then $n(\boldsymbol{r})$ is a complex number. Conventionally, n is parameterized by two real numbers:

$$n =: 1 - \delta + i\beta. \tag{1.30}$$

For thermal neutrons and X-rays, δ and β are almost always nonnegative,[8] and much smaller than 1. This explains why in most scattering geometries the ordinary Born approximation with $\boldsymbol{\Lambda} \equiv 0$ is perfectly adequate. In layered samples under grazing incidence, however, even small differences in n can cause substantial *refraction* and *reflection*. To model GISAS, therefore, it is necessary to use DWBA, and to let $\boldsymbol{\Lambda}$ represent the average vertical refractive index profile $\overline{n}(z)$.

1.2.2 The Rayleigh-Born expansion

The solution of the wave equation (1.26) starts with the determination of the incident wave $\boldsymbol{\Psi}_\text{i}$. It is important to distinguish the *incident* from the *exciting* wave. They coincide in ordinary Born approximation, but not in DWBA.

The *exciting wave* is prepared far outside the sample by a radiation source and some optical devices. It is a superposition of plane waves, as discussed later in the context of instrumental resolution effects (Chapter 4). While discussing scattering theory, it is usually represented by a single plane wave $\boldsymbol{\Psi}_\text{e}(\boldsymbol{r}) = \hat{\boldsymbol{u}}_\text{e}\mathrm{e}^{i\boldsymbol{k}_\text{e}\boldsymbol{r}}$. This function is defined for all $\boldsymbol{r}$, but is physical only along the primary beam, upstream of the sample.

_____

[8]The plus sign in front of $i\beta$ is a consequence of the quantum-mechanical sign convention; in the X-ray crystallography convention it would be a minus sign.

The *incident wave* $\boldsymbol{\Psi}_i$ is an exact solution of (1.28) under the boundary condition that it must match $\boldsymbol{\Psi}_e$ upstream of the sample. Inside the sample it undergoes refraction and reflection or other modifications under the influence of the distortion field $\boldsymbol{\Lambda}$.

A formal solution of the wave equation (1.26) is provided by the *Lippmann-Schwinger equation*

$$\boldsymbol{\Psi}(\boldsymbol{r}) = \boldsymbol{\Psi}_i(\boldsymbol{r}) + \int \mathrm{d}^3 r' \, \boldsymbol{G}(\boldsymbol{r}, \boldsymbol{r}') \boldsymbol{U}(\boldsymbol{r}') \boldsymbol{\Psi}(\boldsymbol{r}'). \tag{1.31}$$

It involves the Green function $\boldsymbol{G}$, which must fulfill

$$\boldsymbol{D}(\boldsymbol{r}) \boldsymbol{G}(\boldsymbol{r}, \boldsymbol{r}') = \mathbf{1}\delta(\boldsymbol{r} - \boldsymbol{r}') =: \boldsymbol{\delta}(\boldsymbol{r} - \boldsymbol{r}'). \tag{1.32}$$

To see that the Lippmann-Schwinger equation solves indeed the perturbed wave equation (1.26), operate on both sides of (1.31) with $\boldsymbol{D}(\boldsymbol{r})$. The Lippmann-Schwinger equation can be resolved into an infinite series by iteratively substituting the full right-hand side of (1.31) for the occurence of $\boldsymbol{\Psi}$ in the integrand. This is the *Born expansion* or *Born series*.[9] Successive terms in this series contain rising powers of $\boldsymbol{U}$. As long as $\boldsymbol{U}$ is a small perturbation, the series converges quickly. In *first-order Born approximation*, only the linear order in $\boldsymbol{U}$ is retained,

$$\boldsymbol{\Psi}(\boldsymbol{r}) = \boldsymbol{\Psi}_i(\boldsymbol{r}) + \int \mathrm{d}^3 r' \, \boldsymbol{G}(\boldsymbol{r}, \boldsymbol{r}') \boldsymbol{U}(\boldsymbol{r}') \boldsymbol{\Psi}_i(\boldsymbol{r}'). \tag{1.33}$$

This is the base for material investigations with X-rays or neutrons, where sample structures that modulate the perturbation potential $\boldsymbol{U}$ are deduced from the scattered intensity $|\boldsymbol{\Psi}(\boldsymbol{r})|^2$. Detectors placed at positions $\boldsymbol{r}$ that are not illuminated by the incident beam only see the scattered wave

$$\boldsymbol{\Psi}_s(\boldsymbol{r}) := \int \mathrm{d}^3 r' \, \boldsymbol{G}(\boldsymbol{r}, \boldsymbol{r}') \boldsymbol{U}(\boldsymbol{r}') \boldsymbol{\Psi}_i(\boldsymbol{r}'). \tag{1.34}$$

For brevity and mathematical convenience, the integral has no bounds and therefore formally runs over the entire space. However, $\boldsymbol{U}(\boldsymbol{r}')$ is nonzero only if $\boldsymbol{r}'$ lies inside the finite sample volume.

1.2.3 Far-field Green function

In experiments, scattered radiation is measured at a detector position $\boldsymbol{r}$ so far outside the sample that the distance from the sample to the detector is must be much larger than the size of the sample. This is just the condition for *Fraunhofer diffraction*; in scattering theory, it is known as the *far-field approximation*. We choose the coordinate origin inside the sample so that the far-field asymptote corresponds to the limit $r \to \infty$.

---

[9]Named after Max Born who introduced it in quantum mechanics. It is actually due to Lord Rayleigh who devised it for sound, and later also applied it to electromagnetic waves, which resulted in his famous explanation of the blue sky.
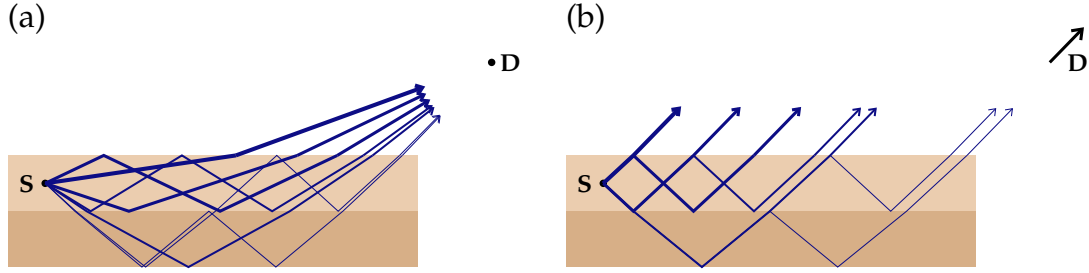
Figure 1.1: (a) The Green function $G(\boldsymbol{r}_{\mathrm{S}}, \boldsymbol{r}_{\mathrm{D}})$ is the probability that radiation emitted by a source S is reaches a detector D. If S is a locus of scattering in a multilayer sample, then G is a sum over different trajectories, involving refraction and reflection at layer interfaces. (b) For the far-field Green function $G^\infty(\boldsymbol{r}_{\mathrm{S}}, \boldsymbol{r}_{\mathrm{D}})$, the detector is moved so far away from the sample that all trajectories are practically parallel when they leave the sample.

To determine the far-field asymptote $\boldsymbol{\Psi}_{\mathrm{s}}^\infty(\boldsymbol{r})$ of the scattered wave $\boldsymbol{\Psi}_{\mathrm{s}}$ from (1.34), it is sufficient to solve (1.32) for the far-field Green function

$$\boldsymbol{G}^\infty(\boldsymbol{r}, \boldsymbol{r}') := \lim_{r \to \infty} \boldsymbol{G}(\boldsymbol{r}, \boldsymbol{r}'). \tag{1.35}$$

This solution is[10]

$$\boldsymbol{G}^\infty(\boldsymbol{r}, \boldsymbol{r}') = \phi(r) \sum_\alpha \hat{\boldsymbol{u}}_\alpha \otimes \boldsymbol{\Psi}_{\hat{\boldsymbol{u}}_\alpha}^*(\boldsymbol{r}'), \tag{1.36}$$

where $\alpha = 1, 2$ is the index of an orthonormal base of polarization vectors $\hat{\boldsymbol{u}}_\alpha$, ϕ is an outgoing spherical wave with

$$\phi(r) := \frac{\mathrm{e}^{iKr}}{4\pi r}, \tag{1.37}$$

and $\boldsymbol{\Psi}_{\hat{\boldsymbol{u}}}$ is a solution of the unperturbed distorted wave equation

$$\boldsymbol{D}(\boldsymbol{r})\boldsymbol{\Psi}_{\hat{\boldsymbol{u}}}(\boldsymbol{r}) = 0 \tag{1.38}$$

with the boundary condition

$$\boldsymbol{\Psi}_{\hat{\boldsymbol{u}}}(\boldsymbol{r}) = \hat{\boldsymbol{u}}\mathrm{e}^{i\boldsymbol{k}_{\mathrm{f}}\boldsymbol{r}} \tag{1.39}$$

for $r \to \infty$ and with an outgoing wavevector $\boldsymbol{k}_{\mathrm{f}} := K\boldsymbol{r}/r$.

We now outline a proof for (1.36). We take for granted that Green functions obye *source-detector reciprocity* [15],

$$\boldsymbol{G}(\boldsymbol{r}, \boldsymbol{r}') = \boldsymbol{G}(\boldsymbol{r}', \boldsymbol{r}). \tag{1.40}$$

We first consider wave propagation in vacuum, denoted by an overset circle. Exact Green functions are known. The far-field must be taken explicitly, and in all cases

$$\boldsymbol{G}_{0\alpha}^\infty(\boldsymbol{r}, \boldsymbol{r}') = \phi(r)\boldsymbol{\Psi}_{0\alpha}^*(\boldsymbol{r}') \tag{1.41}$$

---

[10]To our knowledge, the simple expression (1.36) has never before been stated. Informations about similar results anywhere in the literature would be highly welcome.

is obtained. Following Dietrich and Wagner [13, 14, 16], we write the Lippmann-Schwinger equations for a distorted wave

$$\Psi_{0\alpha}(\boldsymbol{r}) = \int \mathrm{d}^3 r'' \left(\delta(\boldsymbol{r} - \boldsymbol{r}'') + \boldsymbol{G}_{0\alpha}(\boldsymbol{r}, \boldsymbol{r}'')\boldsymbol{\Lambda}(\boldsymbol{r}'') \right) \Psi_{\hat{\boldsymbol{u}}}(\boldsymbol{r}''), \tag{1.42}$$

and for the Green function

$$\boldsymbol{G}_{0\alpha}(\boldsymbol{r}, \boldsymbol{r}') = \int \mathrm{d}^3 r'' \left(\delta(\boldsymbol{r} - \boldsymbol{r}'') + \boldsymbol{G}_{0\alpha}(\boldsymbol{r}, \boldsymbol{r}'')\boldsymbol{\Lambda}(\boldsymbol{r}'') \right) \boldsymbol{G}_{\hat{\boldsymbol{u}}}(\boldsymbol{r}'', \boldsymbol{r}'). \tag{1.43}$$

Operate on both sides with $\boldsymbol{D}_0(\boldsymbol{r})$ to verify that

$$\boldsymbol{D}_0(\boldsymbol{r})\boldsymbol{G}_0(\boldsymbol{r}, \boldsymbol{r}') = \boldsymbol{\delta}(\boldsymbol{r} - \boldsymbol{r}') \text{ and } \boldsymbol{D}_0(\boldsymbol{r})\boldsymbol{\Psi}_0(r) = 0 \tag{1.44}$$

imply

$$\boldsymbol{D}(\boldsymbol{r})\boldsymbol{G}(\boldsymbol{r}, \boldsymbol{r}') = \boldsymbol{\delta}(\boldsymbol{r} - \boldsymbol{r}') \text{ and } \boldsymbol{D}(\boldsymbol{r})\boldsymbol{\Psi}(r) = 0. \tag{1.45}$$

To continue, use the reciprocity of the Green function, and take the far-field limit to transform (1.43) into

$$\phi(\boldsymbol{r}')\boldsymbol{\Psi}_{0\alpha}^*(\boldsymbol{r}) = \int \mathrm{d}^3 r'' \left(\delta(\boldsymbol{r} - \boldsymbol{r}'') + \boldsymbol{G}_{0\alpha}(\boldsymbol{r}, \boldsymbol{r}'')\boldsymbol{\Lambda}(\boldsymbol{r}'') \right) \boldsymbol{G}_{\hat{\boldsymbol{u}}}^\infty(\boldsymbol{r}', \boldsymbol{r}''). \tag{1.46}$$

Take the complex conjugate of (1.42), multiply with $\phi(\boldsymbol{r}')$, and compare with (1.46) to read off

$$\boldsymbol{G}_{\hat{\boldsymbol{u}}}^\infty(\boldsymbol{r}', \boldsymbol{r}'') = \phi(\boldsymbol{r}')\boldsymbol{\Psi}_{\hat{\boldsymbol{u}}}(\boldsymbol{r}''), \tag{1.47}$$

which is (1.36).

1.2.4 Differential cross section

The ratio of the scattered flux hitting an infinitesimal detector area $r^2 \mathrm{d}\Omega$ to the incident flux is expressed as a *differential cross section*

$$\frac{\mathrm{d}\sigma}{\mathrm{d}\Omega} := \frac{r^2 J(\boldsymbol{r})}{J_\mathrm{i}}. \tag{1.48}$$

For a monochromatic plane incident wave **??**, the flux is

$$\boldsymbol{J}_\mathrm{i} = \boldsymbol{k}_\mathrm{i}. \tag{1.49}$$

With the far-field result **??** and the notation **??**, the scattered flux at the detector is

$$\boldsymbol{J}(\boldsymbol{r}) = \hat{\boldsymbol{r}}\frac{K}{r^2}|\langle\psi_\mathrm{i}|\delta v|\psi_\mathrm{f}\rangle|^2. \tag{1.50}$$

Inserting these into definition (1.48), we obtain the generic differential cross section of elastic scattering in first order Born approximation,

$$\frac{\mathrm{d}\sigma}{\mathrm{d}\Omega} = |\langle\psi_\mathrm{i}|\delta v|\psi_\mathrm{f}\rangle|^2. \tag{1.51}$$

As we shall see below, it holds not only for plane waves governed by the Helmholtz equation, but also for distorted waves. In the plane-wave case **??** considered here, the differential cross section is just the squared modulus of the Fourier transform of the SLD,

$$\frac{\mathrm{d}\sigma}{\mathrm{d}\Omega} = |v(\boldsymbol{q})|^2. \tag{1.52}$$

1.3 Coherent vs incoherent scattering

1.3.1 Coherence length

Per (1.51) and **??**, the matrix element $\langle \psi_\mathrm{i} | \delta v | \psi_\mathrm{f} \rangle$ is given by a three-dimensional integral

$$\langle \psi_\mathrm{i} | \delta v | \psi_\mathrm{f} \rangle := \int \mathrm{d}^3 r \, \psi_\mathrm{i}^*(\boldsymbol{r}) \delta v(\boldsymbol{r}) \psi_\mathrm{f}(\boldsymbol{r}). \tag{1.53}$$

The integration domain is effectively limited to a finite z interval, where $\delta v(\boldsymbol{r})$ is nonzero. The horizontal integration domain, however, is infinite within our formalism, which is of course an idealization. Obviously, physical integration limits are imposed by the finite *illuminated sample area*.[11] Another limitation comes from the finite *coherence length* of the instrumental setup, which usually is much shorter than the sample width and length [17, 18].[12]

While each single neutron is described by a wavefunction that allows for *coherent* superposition of different contributions to the scattered wavefunction, the final detector statistics is given by an *incoherent* sum over the differential cross sections of individual neutrons. The finite *resolution* of an experimental setup is in part due to the fact that different neutrons have different wavenumbers, originate[13] at different points in the moderator, and are detected at slightly different points within one detector pixel. This can be modeled by computing expected scattering intensities as averages over different neutrons with K, $\hat{\boldsymbol{k}}_\mathrm{i}$, and $\hat{\boldsymbol{k}}_\mathrm{f}$ drawn at random from appropriate distributions.

However, this is not the full story. In the above introduction to the Born approximation we have made the standard assumption that an incoming neutron can be described by a plane wave $\psi_\mathrm{i} = \mathrm{e}^{i\boldsymbol{k}_\mathrm{i}\boldsymbol{r}}$. The wavefunction ψ_f traced back from the detector is also approximated by a plane wave. In the DWBA we allow these waves to be distorted within the sample, but when impinging on the sample they still are plane. A plane wave obviously is an idealized concept, since it has infinite lateral extension. The *transverse coherence length* indicates the scale beyond which this approximation becomes invalid. At larger scales, the wave fronts appear randomly distorted. Physical causes of these distortions include reflections in the neutron guide, diffraction by guide windows and other slits, and diffraction by imperfect monochromator crystals. Of course the distorted wave still admits a Fourier decomposition into plane waves with slightly different wavevectors. In practice, it is impossible to distinguish this spread of wavevectors from the incoherent spread described in the previous paragraph. The instrumental resolution function therefore accounts for both causes of wavevector distortion.

Usually, therefore, a GISANS image is an incoherent average over coherent diffraction patterns collected from many small subareas of the sample. Only horizontal sample

---

[11]We assume a well aligned instrument, for which the beam footprint and the backtracked detector footprint agree within reasonable accuracy.

[12]These two references also make clear that the theoretical description and the experimental determination of coherence lengths are difficult problems and subject of ongoing research.

[13]It is reasonable to take the last collision in the moderator as the *origin* of a neutron ray, since collisions between neutrons and hydrogen nuclei bound in disordered matter lead to almost perfect decoherence.

structures on scales smaller the coherence length yield interference patterns. Structure fluctuations on larger scales produce said incoherent average of different GISANS images.

The crossover from coherent to incoherent scattering is of course a gradual one. The coherence length indicates where a certain, somewhat arbitrary degree of decoherence is reached. Under these reservations one defines a *coherence spot* in the cross section of an approximately plane wave as an area where the coherence is above a certain threshold. Unless the wave has been prepared in a highly anisotropic guide and slit system, this spot is about circular. Under grazing incidence conditions however, the projection of this spot onto the sample surface yields a very elongated ellipse. Therefore, the coherence length is much larger in x than in y or z direction.[14]

1.3.2 Implementation

Unless otherwise said, BornAgain simulates *coherent* diffraction patterns obtained by the linear superposition of scattered waves. To simulate an *incoherent* mixture of diffraction patterns, the most generic solution is a script with an outer loop that averages over several coherent computations with appropriately distributed parameters.

Currently, BornAgain does not support interferences between particles in different layers.

1.4 OLD STUFF

1.4.1 Vacuum solution

Read as a function of $\boldsymbol{r}$, it is an outgoing spherical wave centered at $\boldsymbol{r}'$. To compute the far-field limit (1.35), we expand for $\boldsymbol{r}'$ with $r' \ll r$:

$$\left|\boldsymbol{r} - \boldsymbol{r}'\right| \doteq \sqrt{r^2 - 2\boldsymbol{r}\,\boldsymbol{r}'} \doteq r - \frac{\boldsymbol{r}\,\boldsymbol{r}'}{r} \equiv r - \frac{\boldsymbol{k}_{\mathrm{f}}\boldsymbol{r}'}{K}, \tag{1.54}$$

where we have introduced the outgoing wavevector $\boldsymbol{k}_{\mathrm{f}} := K\boldsymbol{r}/r$. We apply this to **??**, and obtain in leading order the far-field Green function

$$G_\infty(\boldsymbol{r}, \boldsymbol{r}') = \frac{\mathrm{e}^{iKr}}{4\pi r}\psi_{\mathrm{f}}^*(\boldsymbol{r}'), \tag{1.55}$$

where

$$\psi_{\mathrm{f}}(\boldsymbol{r}) := \mathrm{e}^{i\boldsymbol{k}_{\mathrm{f}}\boldsymbol{r}} \tag{1.56}$$

is a plane wave propagating towards the detector, and ψ^* designates the complex conjugate of ψ. As function of $\boldsymbol{r}$, G_∞ is an outgoing spherical wave. Inserting **??** in (1.34), we obtain the far-field approximation for the scattered wave,

$$\psi_{\mathrm{s}\infty}(\boldsymbol{r}) = \frac{\mathrm{e}^{iKr}}{r}\left\langle \psi_{\mathrm{i}}|\delta v|\psi_{\mathrm{f}}\right\rangle^* \tag{1.57}$$

---

[14]This has nothing to do with the distinction of *transverse* and *longitudinal* coherence length. Longitudinal coherence has to do with wavelength stability and is of no importance for elastic scattering. We are talking here about *horizontal* and *vertical* projections of the *transverse* coherence length.

with the Dirac notation for the scattering matrix element

$$\langle\psi_{\mathrm{i}}|\delta v|\psi_{\mathrm{f}}| := \int \mathrm{d}^3 r\, \psi_{\mathrm{i}}^*(\boldsymbol{r})\delta v(\boldsymbol{r})\psi_{\mathrm{f}}(\boldsymbol{r}). \tag{1.58}$$

Since per **??** and **??** our ψ_{i} and ψ_{f} are plane waves, the matrix element can be simplified as

$$\langle\psi_{\mathrm{i}}|\delta v|\psi_{\mathrm{f}}\rangle = \int \mathrm{d}^3 r\, \mathrm{e}^{-i\boldsymbol{k}_{\mathrm{i}}\boldsymbol{r}}\delta v(\boldsymbol{r})\mathrm{e}^{i\boldsymbol{k}_{\mathrm{f}}\boldsymbol{r}} = \int \mathrm{d}^3 r\, \mathrm{e}^{i\boldsymbol{q}\boldsymbol{r}}\delta v(\boldsymbol{r}) =: v(\boldsymbol{q}), \tag{1.59}$$

with the *scattering vector*[15]

$$\boldsymbol{q} := \boldsymbol{k}_{\mathrm{f}} - \boldsymbol{k}_{\mathrm{i}}. \tag{1.60}$$

?? summarizes the well-known fact that small-angle neutron scattering basically measures the Fourier transform $v(\boldsymbol{q})$ of the SLD.

---

[15]With this choice of sign, $\hbar\boldsymbol{q}$ is the momentum *gained* by the scattered neutron, and *lost* by the sample. In much of the literature the opposite convention is prefered, since it emphasizes the sample physics over the scattering experiment. However, when working with two-dimensional detectors it is highly desirable to express pixel coordinates and scattering vector components with respect to equally oriented coordinate axes, which can only be achieved by the convention (1.60).

2 Multilayer systems

The distorted-wave ansatz of Chapter 1 started from the decomposition **??** of the scattering-length density $v(\boldsymbol{r})$. It was assumed that propagation of distorted waves can be computed analytically for a function $\overline{v}(\boldsymbol{r})$, so that only the remaining fluctuations $\delta v(\boldsymbol{r})$ cause scattering. In this chapter, we consider wave propagation in a multilayer system for which $\overline{v}(\boldsymbol{r}) = \overline{v}(z)$. In Section 2.1 we introduce notation, factorize the wavefunction into an in-plane and a perpendicular function, and derive the notorious four-term DWBA cross section (2.11). In Section 2.2 we specialize to a stack of homogeneous layers, and describe how the vertical wavefunction is computed in BornAgain.

2.1 DWBA for layered samples

Reflectometry and grazing-incidence scattering are designed for the investigation of surfaces, interfaces, and thin layers, or most generically: samples with a $2 + 1$ dimensional structure. By convention, we choose the sample surface to lie in the xy plane, and its normal point out of the sample in positive z direction. In our visualizations, we will always represent the xy plane as *horizontal*, and the z axis as upward *vertical*, altough there are "horizontal" reflectometers where the sample normal is horizontal in laboratory space.

Scattering from such systems will be studied in distorted-wave Born approximation. To determine the neutron scattering cross section (1.51), we need to determine the incident and final wavefunctions ψ_{i} and ψ_{f}. Vertical variations of the refractive index $n(z)$ cause refraction and reflection. For waves propagating at small glancing angles, the reflectance can take any value between 0 and 1, even though $1 - n$ is only of the order 10^{-5} or smaller. Such zeroth-order effects cannot be accounted for by perturbative scattering theory. Instead, we need to deal with refraction and reflection from the onset, in the wave propagation equation. Accordingly, the SLD decomposition **??** takes the form

$$v(\boldsymbol{r}) = \overline{v}(z) + \delta v(\boldsymbol{r}), \tag{2.1}$$

and the homogeneous wave equation **??** becomes

$$\left\{ \boldsymbol{\nabla}^2 + k(z)^2 \right\} \psi(\boldsymbol{r}) = 0. \tag{2.2}$$
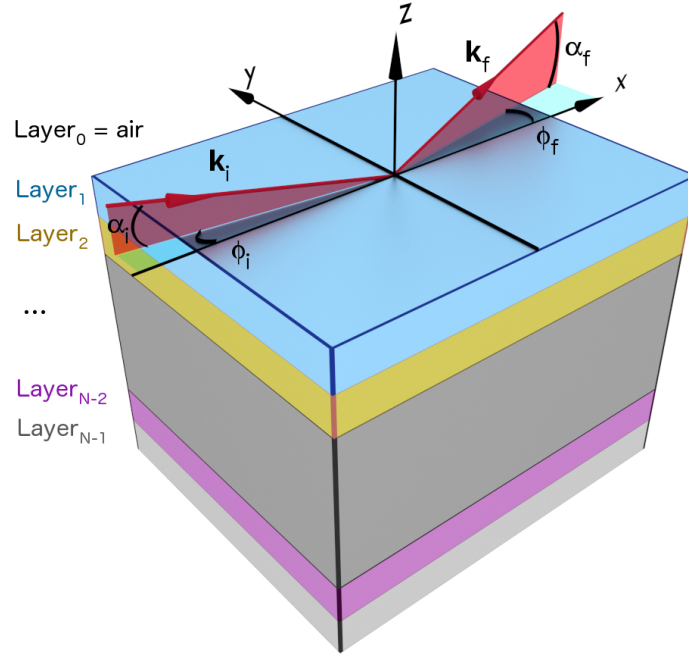
Figure 2.1: Geometric conventions in GISAS scattering comprise a Cartesian coordinate system and a set of angles. The coordinate system has a z axis normal to the sample plane, and pointing into the halfspace where the beam comes from. The x axis usually points along the incident beam, projected onto the sample plane. Incident and final plane waves are characterized by wavevectors $\boldsymbol{k}_{\mathrm{i}}$, $\boldsymbol{k}_{\mathrm{f}}$; the angle α_{i} is the incident glancing angle; ϕ_{i} is usually zero, unless used to describe a sample rotation; α_{f} is the exit angle with respect to the sample's surface; and ϕ_{f} is the scattering angle with respect to the scattering plane. In the above figure ϕ_{f} is negative by convention, while all other angles are positive. The numbered layers illustrate a multilayer system as dicussed in Chapter 2.

Below and above the sample, $k(z) = \mathrm{const}$: in these regions, $\psi(\boldsymbol{r})$ is a superposition of plane waves. The exciting wavefunction is

$$\psi_{\mathrm{e}}(\boldsymbol{r}) = \mathrm{e}^{i\boldsymbol{k}_{\|}\boldsymbol{r}_{\|} + ik_{\perp\mathrm{e}}z}, \tag{2.3}$$

The subscripts $\|$ and $\perp$ refer to the sample xy plane. The wavevector components $\boldsymbol{k}_{\|}$ and $k_{\perp}$ must fulfill

$$k(z)^2 = \boldsymbol{k}_{\|}^2 + k_{\perp}^2. \tag{2.4}$$

Continuity across the sample implies

$$\boldsymbol{k}_{\|} = \mathrm{const.} \tag{2.5}$$

When the incident wave hits the sample, it is wholly or partly reflected. Therefore, the full the solution of (2.2) in the half space of the radiation source is

$$\psi(\boldsymbol{r}) = \mathrm{e}^{i\boldsymbol{k}_{\|}\boldsymbol{r}_{\|} + ik_{\perp\mathrm{e}}z} + R\,\mathrm{e}^{i\boldsymbol{k}_{\|}\boldsymbol{r}_{\|} - ik_{\perp\mathrm{e}}z} \tag{2.6}$$

vacuum / air $\langle\psi_i^-|\delta v|\psi_f^+\rangle$ $\langle\psi_i^-|\delta v|\psi_f^-\rangle$ $\langle\psi_i^+|\delta v|\psi_f^+\rangle$ $\langle\psi_i^+|\delta v|\psi_f^-\rangle$

decorated layer

substrate   term 1   term 2   term 3   term 4
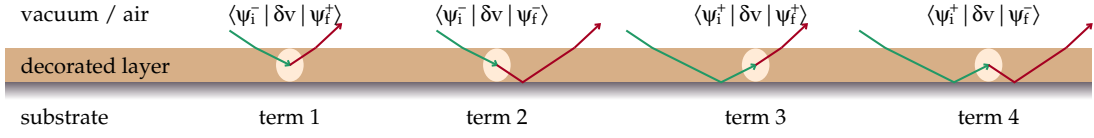
Figure 2.2: The four terms in the DWBA scattering matrix element (2.12). Note that this is a highly simplified visualization. In particular, it does not show multiple reflections of incoming or scattered radiation, though they are properly accounted for by DWBA theory and by all simulation software.

with a complex reflection coefficient R. The reflected flux is given by the reflectance $|R|^2$. In the opposite halfspace, the solution of (2.2) is simply

$$\psi(\boldsymbol{r}) = T\,\mathrm{e}^{i\boldsymbol{k}_\| \boldsymbol{r}_\| + ik_{\perp e}z} \tag{2.7}$$

with a complex transmission coefficient T. The transmitted flux is given by the transmittance $|T|^2$.

Within the sample, the wave equation (2.2) is solved by the factorization ansatz

$$\psi(\boldsymbol{r}) = \mathrm{e}^{i\boldsymbol{k}_\| \boldsymbol{r}_\|}\phi(z). \tag{2.8}$$

The vertical wavefunction $\phi(z)$ is governed by the one-dimensional wave equation

$$\left\{\partial_z^2 + k(z)^2 - k_\|^2\right\}\phi(z) = 0. \tag{2.9}$$

As solution of a differential equation of second degree, $\phi(z)$ can be written as superposition of a downward travelling wave $\phi^-(z)$ and an upward travelling wave $\phi^+(z)$. Accordingly, the three-dimensional wavefunction can be written as

$$\psi(\boldsymbol{r}) = \psi^-(\boldsymbol{r}) + \psi^+(\boldsymbol{r}). \tag{2.10}$$

All this holds not only for the incident wavefunction ψ_i, but also for the wavefunction ψ_f that is tracked back from a detector pixel towards the sample. Therefore the scattering matrix element involves two incident and two final partial wavefunctions. The resulting sum

$$\langle\psi_i|\delta v|\psi_f\rangle = \langle\psi_i^-|\delta v|\psi_f^-\rangle + \langle\psi_i^-|\delta v|\psi_f^+\rangle + \langle\psi_i^+|\delta v|\psi_f^-\rangle + \langle\psi_i^+|\delta v|\psi_f^+\rangle \tag{2.11}$$

is depicted in Figure 2.2. It can be written in an obvious shorthand notation

$$\langle\psi_i|\delta v|\psi_f\rangle = \sum_{\pm_i}\sum_{\pm_f}\langle\psi_i^\pm|\delta v|\psi_f^\pm|. \tag{2.12}$$

This equation contains the essence of the DWBA for GISAS, and is the base for all scattering models implemented in BornAgain. Since $\langle\psi_i|\delta v|\psi_f\rangle$ appears as a squared modulus in the differential cross section (1.51), the four terms of (2.12) can interfere with each other, which adds to the complexity of GISAS patterns.
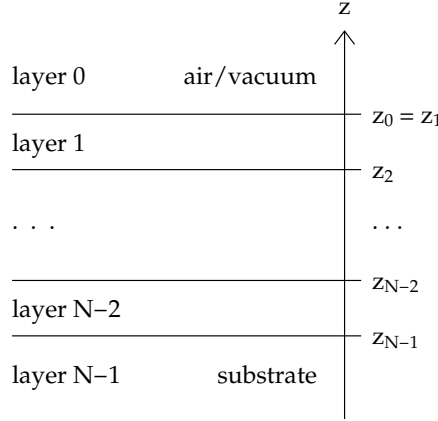
Figure 2.3: Conventions for layer numbers and interface coordinates. A sample has N layers, including the semi-infinite bottom and top layers. Layers are numbered from top to bottom. The top vacuum (or air) layer (which extends to $z \to +\infty$) has number 0, the substrate (extending to $z \to -\infty$) is layer $N - 1$. The parameter z_l is the z coordinate of the *top* interface of layer l, except for z_0 which is the coordinate of the *bottom* interface of the air or vacuum layer 0.

BornAgain supports multilayer samples with refractive index discontinuities at layer interfaces. Conventions for layer numbers and interface coordinates are introduced in Figure 2.3. A sample has N layers, including the semi-infinite bottom and top layers. Numbering is from top to bottom, and from 0 to $N - 1$ as imposed by the programming languages C++ and Python. Each layer l has a constant refractive index n_l and a constant wavenumber $k_l := K_{\text{vac}} n_l$. Any up- or downward travelling solution of the wave equation shall be written as a sum over partial wavefunctions,

$$\psi^{\pm}(\boldsymbol{r}) = \sum_l \psi_l^{\pm}(\boldsymbol{r}), \tag{2.13}$$

with the requirement

$$\psi_l^{\pm}(\boldsymbol{r}) = 0 \text{ for } \boldsymbol{r} \text{ outside layer } l. \tag{2.14}$$

The DWBA matrix element (2.12) then takes the form

$$\langle \psi_{\text{i}} | \delta v | \psi_{\text{f}} \rangle = \sum_l \sum_{\pm_{\text{i}}} \sum_{\pm_{\text{f}}} \langle \psi_{\text{i}l}^{\pm} | \delta v | \psi_{\text{f}l}^{\pm} \rangle . \tag{2.15}$$

All the above can be easily transcribed to electromagnetic waves. The scattering matrix element **??** becomes a four-term some over field components $\boldsymbol{E}_{\text{i},f}^{\pm}$. In full analogy with (2.15), the sum over layers is

$$\langle \boldsymbol{E}_{\text{i}} | \delta v | \boldsymbol{E}_{\text{f}} \rangle = \sum_l \sum_{\pm_{\text{i}}} \sum_{\pm_{\text{f}}} \langle \boldsymbol{E}_{\text{i}l}^{\pm} | \delta v | \boldsymbol{E}_{\text{f}l}^{\pm} \rangle . \tag{2.16}$$

2.2 Homogeneous layers

2.2.1 DWBA for one layer

BornAgain currently only supports layers with a homogenous matrix. In terms of (2.1) this means that $\overline{v}(z) =: v_l$ must be constant within a layer.

Within the layer, the directional neutron wavefunction $\psi_l^\pm$ is a plane wave and factorizes as in (2.8). Its amplitude $A_l^\pm$ is determined recursively by Fresnel's transmission and reflection coefficients that are based on continuity conditions at the layer interfaces. This will be elaborated in Section 2.2.2. The vertical wavenumber is determined by (2.3) and (2.5),

$$k_{\perp l}^\pm = \pm\sqrt{k_l^2 - k_\parallel^2}. \tag{2.17}$$

In the absence of absorption and above the critical angle, wavevectors are real so that we can describe the beam in terms of a glancing angle

$$\alpha_l := \arctan(k_{\perp l}/k_\parallel). \tag{2.18}$$

Equivalently,

$$k_\parallel = K n_l \cos\alpha_l. \tag{2.19}$$

Since $k_\parallel$ is constant across layers, we have

$$n_l \cos\alpha_l = \text{the same for all } l, \tag{2.20}$$

which is Snell's refraction law. In general, however, the vertical wavenumber $k_\perp$, determined by k_l and $k_\parallel$ as per (2.3), can become imaginary (total reflection conditions) or complex (absorbing layer). In these cases, glancing angles are no longer well defined, and the geometric interpretation of $\psi_l(\boldsymbol{r})$ less obvious. so that one has to fully rely on the algebraic formalism.

With the indicator function

$$\chi_l(\boldsymbol{r}) := \begin{cases} 1 & \text{if } z_l \leq z \leq z_{l+1}, \\ 0 & \text{otherwise,} \end{cases} \tag{2.21}$$

the vertical wavefunction can be written

$$\phi_l^\pm(z) = A_l^\pm \mathrm{e}^{\pm ik_{\perp l}(z-z_l)}\chi_l(z). \tag{2.22}$$

The offset z_l has been included in the phase factor for later convenience.

The DWBA transition matrix element (2.12) is

$$\langle\psi_\mathrm{i}|\delta v|\psi_\mathrm{f}\rangle = \sum_l \sum_{\pm_\mathrm{i}} \sum_{\pm_\mathrm{f}} A_{\mathrm{i}l}^{\pm *} A_{\mathrm{f}l}^\pm \delta v_l(\boldsymbol{k}_{\mathrm{f}l}^\pm - \boldsymbol{k}_{\mathrm{i}l}^\pm) \tag{2.23}$$

with the Fourier transform of the SLD restricted to layer l

$$\delta v_l(\boldsymbol{q}) := \int_{z_l}^{z_{l-1}} \mathrm{d}z \int \mathrm{d}^2 r_\parallel \, \mathrm{e}^{i\boldsymbol{q}\boldsymbol{r}} \delta v(\boldsymbol{r}) = \int \mathrm{d}^3 r \, \mathrm{e}^{i\boldsymbol{q}\boldsymbol{r}} \delta v(\boldsymbol{r}) \chi_l(z). \tag{2.24}$$

To alleviate later calculations, we number the four DWBA terms from 1 to 4 as shown in Fig. 2.2, and define the corresponding wavenumbers and amplitude factors and as

$$
\begin{aligned}
\boldsymbol{q}^1 &:= \boldsymbol{k}_{\mathrm{f}}^+ - \boldsymbol{k}_{\mathrm{i}}^-, & C^1 &:= A_{\mathrm{i}}^{-*} A_{\mathrm{f}}^+, \\
\boldsymbol{q}^2 &:= \boldsymbol{k}_{\mathrm{f}}^- - \boldsymbol{k}_{\mathrm{i}}^-, & C^2 &:= A_{\mathrm{i}}^{-*} A_{\mathrm{f}}^-, \\
\boldsymbol{q}^3 &:= \boldsymbol{k}_{\mathrm{f}}^+ - \boldsymbol{k}_{\mathrm{i}}^+, & C^3 &:= A_{\mathrm{i}}^{+*} A_{\mathrm{f}}^+, \\
\boldsymbol{q}^4 &:= \boldsymbol{k}_{\mathrm{f}}^- - \boldsymbol{k}_{\mathrm{i}}^+, & C^4 &:= A_{\mathrm{i}}^{+*} A_{\mathrm{f}}^-.
\end{aligned}
\tag{2.25}
$$

Accordingly, we can write (2.23) as

$$\langle \psi_{\mathrm{i}} | \delta v | \psi_{\mathrm{f}} \rangle = \sum_l \sum_u C_l^u \delta v_l(\boldsymbol{q}_l^u). \tag{2.26}$$

Since $\boldsymbol{k}_\parallel = \mathrm{const}$, all wavevectors $\boldsymbol{q}_l^u$ have the same horizontal component $\boldsymbol{q}_\parallel$; they differ only in their vertical component $q_{l\perp}^u$.

2.2.2 Wave amplitudes

The plane-wave amplitudes $A_{wl}^\pm$ need to be computed recursively from layer to layer. Since these computations are identical for incident and final waves, we omit the subscript w in the remainder of this section. At layer interfaces, the optical potential changes discontinuously. From elementary quantum mechanics we know that piecewise solutions of the Schrödinger equations must be connected such that the wavefunction $\phi(\boldsymbol{r})$ and its first derivative $\boldsymbol{\nabla}\phi(\boldsymbol{r})$ evolve continuously.

Support for rough interfaces is already implemented in BornAgain, but documentation is adjourned to a later edition of this manual.

To deal with the coordinate offsets introduced in (2.22), we introduce the function

$$d_l := z_l - z_{l+1}, \tag{2.27}$$

which is the thickness of layer l, except for $l = 0$, where the special definition of z_0 (Fig. 2.3) implies $d_0 = 0$. We consider the interface between layers l and $l-1$, with $l = 1, \ldots, N-1$, as shown in Fig. 2.4. This interface has the vertical coordinate $z_l = z_{l-1} - d_{l-1}$. Accordingly, the continuity conditions at the interface are

$$
\begin{aligned}
\phi_l(z_l) &= \phi_{l-1}(z_{l-1} - d_{l-1}), \\
\partial_z \phi_l(z_l) &= \partial_z \phi_{l-1}(z_{l-1} - d_{l-1}).
\end{aligned}
\tag{2.28}
$$

We abbreviate

$$f_l := k_{\perp l}/K = \sqrt{n_l^2 - (k_\parallel/K)^2} \tag{2.29}$$
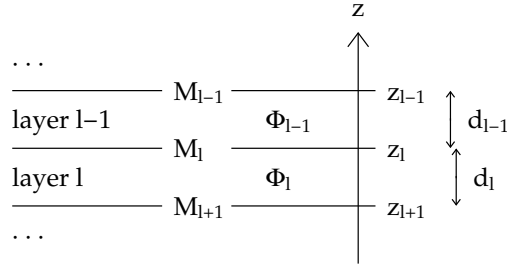
Figure 2.4: The transfer matrix M_l connects the wavefunctions Φ_l, Φ_{l-1} in adjacent layers.

and

$$\delta_l := e^{iKf_ld_l}. \tag{2.30}$$

For the plane waves (2.22), the continuity conditions (2.28) take the form

$$
\begin{aligned}
+A_l^- +A_l^+ &= +A_{l-1}^-\delta_{l-1} \quad +A_{l-1}^+\delta_{l-1}^{-1}, \\
-A_l^- f_l+A_l^+ f_l &= -A_{l-1}^-\delta_{l-1}f_{l-1}+A_{l-1}^+\delta_{l-1}^{-1}f_{l-1}.
\end{aligned}
\tag{2.31}
$$

After some lines of linear algebra, we can rewrite this equation system as

$$\begin{pmatrix} A_{l-1}^- \\ A_{l-1}^+ \end{pmatrix} = M_l \begin{pmatrix} A_l^- \\ A_l^+ \end{pmatrix} \tag{2.32}$$

with the transfer matrix[1]

$$M_l := \begin{pmatrix} \delta_{l-1}^{-1} & 0 \\ 0 & \delta_{l-1} \end{pmatrix} \frac{1}{2f_{l-1}} \begin{pmatrix} (f_{l-1}+f_l) & (f_{l-1}-f_l) \\ (f_{l-1}-f_l) & (f_{l-1}+f_l) \end{pmatrix}. \tag{2.33}$$

In a scattering setup, plane-wave amplitudes are subject to two boundary conditions. Let us assume that the source or the sink is located at $z > 0$. Then in the top layer, $A_0^- = 1$ is given by the incident or back-traced final plane wave. In the substrate, $A_{N-1}^+ = 0$ because there is no radiation coming from $z \to -\infty$. This leaves us with two unkown amplitudes, the overall coefficients of transmission A_{N-1}^- and reflection A_0^+. These two unknowns are connected by a system of two linear equations,

$$\begin{pmatrix} 1 \\ A_0^+ \end{pmatrix} = M_1 \cdots M_{N-1} \begin{pmatrix} A_{N-1}^- \\ 0 \end{pmatrix}. \tag{2.34}$$

---

[1]This approach is generally attributed to Abelès, who elaborated it in his thesis from 1949, published 1950. The usually cited paper [19] is no more than a short advertisement. Parratt [20], unaware of Abelès, expressed the same relation as a recursion formula.

While it is possible in principle to solve this as a matrix equation, the actual implementation in BornAgain[2] starts with a unit vector in the substrate, and then carries out the propagation step (2.32) interface by interface, yielding unnormalized amplitudes

$$
\begin{pmatrix} \tilde{A}_l^- \\ \tilde{A}_l^+ \end{pmatrix} := M_{l+1} \cdots M_{N-1} \begin{pmatrix} 1 \\ 0 \end{pmatrix}.
\tag{2.35}
$$

When the top layer is reached, the obtained values are normalized so that the boundary condition $A_0^- = 1$ be satisfied,

$$
A_l^\pm = \frac{\tilde{A}_l^\pm}{\tilde{A}_0^-}.
\tag{2.36}
$$

For GISAS detection in transmission geometry (sink location $z < 0$) all the development following (2.33) holds with exchanged order of layers: $(0, \ldots, N-1) \mapsto (N-1, \ldots, 0)$.

GISAS in transmission geometry is not yet implemented in BornAgain, but high on our agenda.

The above algorithm fails if $f_l \to 0$ because M_{l+1} becomes singular. The general solution of (2.9) will be a linear function of z:

$$
\phi_l(z) = A_l^0 + A_l^1 z.
\tag{2.37}
$$

In BornAgain, such a linear wavefunction amplitude can not be handled by the form factors, which are only defined in terms of plane waves with complex wavevector components. The following cases are treated seperately:

- There is only one layer: this is a trivial case whithout any need to calculate wave coefficients. The solution in the single layer is just the incoming/outgoing plane wave.

- The top layer of a multilayer has $f_0 = 0$: the limit $f_0 \to 0$ is well-defined and the solution is given by $A_0^+ = -A_0^-$ and $A_l^\pm = 0$ for $l > 0$.

- $f_l = 0$ for a layer with $l > 0$: In this case f_l will be given a very small imaginary value, representing a slight absorption. However, this should be inconsequential because the index of refraction of non-vacuum layer always contains an absorptive component.

2.2.3 Flux, evanescent waves

We write

$$
k_\perp =: k_\perp' + i k_\perp''
\tag{2.38}
$$

---

[2]In file SpecularMatrix.cpp, function `SpecularMatrix::execute`.

for the decomposition into a real and an imaginary part. Accordingly, full wavevectors have the decomposition

$$\boldsymbol{k}^{\pm} =: \boldsymbol{k}^{\pm\prime} + i\boldsymbol{k}^{\pm\prime\prime} = \boldsymbol{k}_{\parallel} \pm (k'_{\perp} + ik''_{\perp})\hat{\boldsymbol{z}}. \tag{2.39}$$

Per (1.30), we have $\beta \geq 0$ and $\delta < 1$, from which it follows that $k''_{\perp}$ always has the same sign as $k'_{\perp}$.

After these preparations, we can compute the flux **??**:

$$\begin{aligned}
\boldsymbol{J}(\boldsymbol{r}) = |A^{-}|^2\, \mathrm{e}^{+2k''_{\perp}(z-z_l)}\boldsymbol{k}^{-\prime} + |A^{+}|^2\, \mathrm{e}^{-2k''_{\perp}(z-z_l)}\boldsymbol{k}^{+\prime} \\
+ \left[A^{-}A^{+*}\mathrm{e}^{-2ik'_{\perp}(z-z_l)}\left(\boldsymbol{k}_{\parallel} - ik''_{\perp}\hat{\boldsymbol{z}} \right) + \mathrm{c.c.} \right].
\end{aligned} \tag{2.40}$$

The first two terms describe the exponential intensity decrease due to absorption, while the oscillatory term in square brackets is responsible for waveguide effects in layers with finite thickness. The flux can also be written in terms of the one-dimensional wavefunctions $\phi^{\pm}(z)$:

$$\begin{aligned}
\boldsymbol{J}(\boldsymbol{r}) = |\phi^{+}(z) + \phi^{-}(z)|^2 \cdot \boldsymbol{k}_{\parallel} \\
+ \left[|\phi^{+}(z)|^2\, k'_{\perp} - |\phi^{-}(z)|^2\, k'_{\perp} + 2\,\mathrm{Im}(\phi^{-}(z)\phi^{+*}(z))k''_{\perp} \right] \cdot \hat{\boldsymbol{z}}.
\end{aligned} \tag{2.41}$$

The first term denotes the horizontal component of the flux and can be seen to consist of the product of the particle density at position z and the wavector $\boldsymbol{k}_{\parallel}$. The z-component consists of the difference between the up- and downward travelling wave components and an extra term that encodes the interference between them.

In the special case of a purely imaginary $k_{\perp l}$, the flux becomes:

$$\boldsymbol{J}(\boldsymbol{r}) = |\psi|^2\, \boldsymbol{k}_{\parallel} + 2\,\mathrm{Im}(A^{-}A^{+*})k''_{\perp}\hat{\boldsymbol{z}}. \tag{2.42}$$

This flux consists of two clearly distinct parts: an *evanescent wave*, travelling horizontally and a vertical component that is independent of the z position. The vertical component is a necessary degree of freedom to fulfill the boundary conditions at the layer's top and bottom interfaces. In the case of a semi-infinite layer, the vertical component becomes zero and all incoming radiation at the top of the layer undergoes *total reflection*.

2.2.4 Modifications for X-rays

We shall now translate the above results from unpolarized neutrons to X-rays. The vectorial amplitude of the electromagnetic field will require nontrivial modifications. In place of the factorization (2.8), we write

$$\boldsymbol{E}(\boldsymbol{r}) = \mathrm{e}^{i\boldsymbol{k}_{\parallel}\boldsymbol{r}}\boldsymbol{\Phi}(z). \tag{2.43}$$

In place of (2.22), the vertical wavefunction is

$$\boldsymbol{\Phi}_l^{\pm}(z) = \boldsymbol{A}_l^{\pm}\mathrm{e}^{\pm ik_{\perp}(z-z_l)}\chi_l(z). \tag{2.44}$$
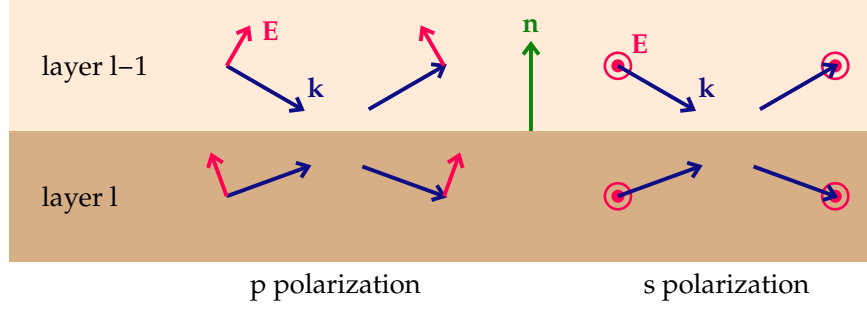
Figure 2.5: Conventions for polarization directions relative to a refracting interface: For p polarization, the electric field vector $\boldsymbol{E}$ is parallel to the interface normal $\boldsymbol{n}$; for s polarization, it is perpendicular (*senkrecht* in German). In either case, $\boldsymbol{E}$ is perpendicular to the wavevector $\boldsymbol{k}$.

The vectorial character of $\boldsymbol{A}_{wl}^{\pm}$ will require changes in Sec. 2.2.2. For electromagnetic radiation in nonmagnetic media, the boundary conditions at an interface with normal $\boldsymbol{n}$ are [21, eq. 7.37]

$$\sum_{\pm} \bar{\epsilon}\, \boldsymbol{E}^{\pm}\, \boldsymbol{n} = \text{const}, \tag{2.45}$$

$$\sum_{\pm} \boldsymbol{E}^{\pm} \times \boldsymbol{n} = \text{const}, \tag{2.46}$$

$$\sum_{\pm} \boldsymbol{k}_l^{\pm} \times \boldsymbol{E}^{\pm} = \text{const}. \tag{2.47}$$

We will only consider the two polarization directions, conventionally designated as p and s, defined in Figure 2.5. As some algebra on (2.45) to (2.47) would show, these are *principal* axes, meaning that if both incoming fields $\boldsymbol{E}_{l-1}^{-}$ and $\boldsymbol{E}_l^{+}$ are strictly polarized in either p or s direction, then the outgoing fields $\boldsymbol{E}_{l-1}^{+}$ and $\boldsymbol{E}_l^{-}$ are polarized in the same direction. Conversely, if the incoming fields are mixtures of p and s polarization, then the outgoing fields will be, in general, mixed differently. Therefore if polarization factors are quantitatively important in an experiment, one should strive to accurately polarize the incident beam in p or s direction in order to avoid the extra complication of variably mixed polarizations.

Further algebra on (2.45) to (2.47) replicates the reflection law that relates $\boldsymbol{k}^{-}$ and k^{+} and Snell's law (2.20). Taking these for granted, we only retain equations that are needed to determine the field amplitudes $E^{\pm}$. For p polarization they yield

$$\begin{pmatrix} k & k \\ -k_{\perp}/k & k_{\perp}/k \end{pmatrix} \begin{pmatrix} E^{-} \\ E^{+} \end{pmatrix} = \text{const}, \tag{2.48}$$

and for s polarization

$$\begin{pmatrix} 1 & 1 \\ -k_{\perp} & k_{\perp} \end{pmatrix} \begin{pmatrix} E^{-} \\ E^{+} \end{pmatrix} = \text{const}. \tag{2.49}$$

The latter equation can be brought into the form (2.31). In consequence, s-polarized X-rays are refracted and reflected in exactly the same ways as unpolarized neutrons. For p polarization, the transfer matrix (2.33) must be replaced by

$$M_l^{(p)} = TODO, \tag{2.50}$$

In BornAgain, this modified transfer matrix is not yet implemented; only s polarized X-rays are currently supported.

The following paragraph on polarization factors shall be worked out next:

In s geometry the coefficients C_l^u of Equation (2.51) are given by simple products of scalar amplitudes as in (2.25).

The DWBA matrix element is

$$\langle \boldsymbol{E}_\mathrm{i} | \delta v | \boldsymbol{E}_\mathrm{f} \rangle = \sum_l \sum_u C_l^u \delta v_l(\boldsymbol{q}_l^u). \tag{2.51}$$

in full analogy with (2.26), but the coefficients are now scalar products $C^1 = \boldsymbol{A}_\mathrm{i}^{-*} \boldsymbol{A}_\mathrm{f}^+$ etc. instead of the products of scalar factors in (2.25).

and the coefficients of Equation (2.51) are

$$\begin{aligned}
C^1 &= A_\mathrm{i}^{-*} A_\mathrm{f}^+, \\
C^2 &= A_\mathrm{i}^{-*} A_\mathrm{f}^- \cos(\alpha_- + \alpha_+), \\
C^3 &= A_\mathrm{i}^{+*} A_\mathrm{f}^+ \cos(\alpha_- + \alpha_+), \\
C^4 &= A_\mathrm{i}^{+*} A_\mathrm{f}^- .
\end{aligned} \tag{2.52}$$

In BornAgain, polarization factors are not yet implemented.

3 Particle Assemblies

3.1 Generic scattering cross section

In many important GISAS applications, fluctuations of the refractive index are due to *droplets*, *islands*, *inclusions* or *holes* of a mesoscopic size (nanometer to micrometer). In the following, all such inhomogeneities will be described as *particles* that are embedded in a material layer. In BornAgain, a sample can be decorated with an arbitrary number of different particles species. For readability, in the following only *one* kind of embedded particles will be considered; the generalization to several species is straightforward.

The matrix material has a SLD $v_{\mathrm{m}}(z)$ that may or may not vary with z. The SLD of the entire sample, consisting of the matrix and an assembly of particles of type p, shall be written

$$v(\boldsymbol{r}) = v_{\mathrm{m}}(z) + \Delta v_{\mathrm{p}}(\boldsymbol{r}). \tag{3.1}$$

If the particles are homogeneous, then

$$\Delta v_{\mathrm{p}}(\boldsymbol{r}) = (v_{\mathrm{p}} - v_{\mathrm{m}}(z)) \, \chi_{\mathrm{p}}(\boldsymbol{r}) \tag{3.2}$$

with the indicator function

$$\chi_{\mathrm{p}}(\boldsymbol{r}) := \begin{cases} 1 & \text{if } \boldsymbol{r} \text{ in p,} \\ 0 & \text{otherwise.} \end{cases} \tag{3.3}$$

The following formalism, however, shall not rely on (3.2), but also allow for soft particles for which $\Delta v_{\mathrm{p}}(\boldsymbol{r})$ is a continuous function of $\boldsymbol{r}$.

The sum (3.1) has the same form as the decomposition (2.1). Nonetheless, implementations are free to choose a convenient mean SLD $\overline{v}(z)$. Currently, BornAgain uses $\overline{v}(z) := v_{\mathrm{m}}(z)$, though we suspect that for non-dilute particles $\overline{v}(z) := v_{\mathrm{m}}(z) + \overline{\Delta v_{\mathrm{p}}(\boldsymbol{r})}$ would yield a more accurate scattering simulation. With $\overline{v}(z) := v_{\mathrm{m}}(z)$, we have $\delta v_l(\boldsymbol{r}) = \Delta v_{\mathrm{p}}(\boldsymbol{r})$. Outside the layer that contains the embedded particles, $\delta v_l(\boldsymbol{r}) = 0$.

With the factorization (2.8), the scattering matrix element **??** becomes

$$\langle \psi_{\mathrm{i}} | \delta v | \psi_{\mathrm{f}} \rangle = \int \mathrm{d}^2 r_{\parallel} \, \mathrm{e}^{i \boldsymbol{q}_{\parallel} \boldsymbol{r}_{\parallel}} \int \mathrm{d}z \, \phi_{\mathrm{i}}^*(z) \delta v(\boldsymbol{r}) \phi_{\mathrm{f}}(z). \tag{3.4}$$

The SLD distribution of a set of identical particles, located at positions $\boldsymbol{R}_j$, can be written as a sum

$$v_{\mathrm{p}}(\boldsymbol{r}) = \sum_j F(\boldsymbol{r} - \boldsymbol{R}_j). \tag{3.5}$$

In many applications, particles are not all identical. They may vary in shape, size, orientation, or refractive index profile. These degrees of freedom shall be denoted by a parameter vector $\boldsymbol{T}_j$. Specifically for a $2 + 1$ dimensional sample, it is convenient to restrict the coordinate vectors $\boldsymbol{R}_j$ to the xy plane, and to redefine $\boldsymbol{T}_j$ to include the vertical particle component of $\boldsymbol{R}_j$. In consequence, (3.5) is replaced by

$$v_{\mathrm{p}}(\boldsymbol{r}) = \sum_j F(\boldsymbol{r} - \boldsymbol{R}_{j\|}, \boldsymbol{T}_j). \tag{3.6}$$

With the *DWBA form factor*

$$\mathcal{F}_{\mathrm{if}}(\boldsymbol{q}_\|, \boldsymbol{T}) := \int \mathrm{d}^2 r_\| \, \mathrm{e}^{i\boldsymbol{q}_\| \boldsymbol{r}_\|} \int \mathrm{d}z \, \phi_{\mathrm{i}}^*(z) F(\boldsymbol{r}, \boldsymbol{T}) \phi_{\mathrm{f}}(z), \tag{3.7}$$

the scattering matrix element (3.4) becomes

$$\langle \psi_{\mathrm{i}} | \delta v | \psi_{\mathrm{f}} \rangle = \sum_j \mathrm{e}^{i\boldsymbol{q}_\| \boldsymbol{R}_{j\|}} \mathcal{F}_{\mathrm{if}}(\boldsymbol{q}_\|, \boldsymbol{T}_j). \tag{3.8}$$

The elastic scattering cross section (1.51) can be written as

$$\frac{\mathrm{d}\sigma}{\mathrm{d}\Omega} = \sum_{jk} \mathrm{e}^{i\boldsymbol{q}_\| (\boldsymbol{R}_{j\|} - \boldsymbol{R}_{k\|})} \mathcal{F}_{\mathrm{if}}(\boldsymbol{q}_\|, \boldsymbol{T}_j) \mathcal{F}_{\mathrm{if}}^*(\boldsymbol{q}_\|, \boldsymbol{T}_k). \tag{3.9}$$

In the following Section 3.2 we discuss the form factor $\mathcal{F}_{\mathrm{if}}$. The remainder of this chapter is devoted to the positional term and to the coupling between particle form and position; various approximations are used to make (3.8) manageable.

3.2 Particle form factor

To compute the DWBA form factor for a generic vertical wavefunction $\phi(z)$, it is advantageous to exchange the order of integration in (3.7):

$$\mathcal{F}_{\mathrm{if}}(\boldsymbol{q}_\|, \boldsymbol{T}) = \int \mathrm{d}z \, \phi_{\mathrm{i}}^*(z) F(q_\|, z, \boldsymbol{T}) \phi_{\mathrm{f}}(z). \tag{3.10}$$

The function

$$F(\boldsymbol{q}_\|, z, \boldsymbol{T}) := \int \mathrm{d}^2 r_\| \, \mathrm{e}^{i\boldsymbol{q}_\| \boldsymbol{r}_\|} F(\boldsymbol{r}, \boldsymbol{T}) \tag{3.11}$$

is an *intermediate Fourier transform*, since it is a transform in some, but not all the coordinates; more specifically, it may be called the *horizontal Fourier transform*. For homogeneous particles, it is the *shape transform* of horizontal cuts.

For samples that only consist of homogeneous layers the wavefunction is the sum of two plane waves (2.22). With the notations (2.25), the DWBA form factor (3.10) becomes

$$\mathcal{F}_{\mathrm{if}}(\boldsymbol{q}_\|, \boldsymbol{T}) = \sum_l \sum_u C_l^u F_l(\boldsymbol{q}_l^u, \boldsymbol{T}) \tag{3.12}$$

with

$$F_l(\boldsymbol{q}, \boldsymbol{T}) \coloneqq \int \mathrm{d}z \, \mathrm{e}^{iq_\perp z} F(\boldsymbol{q}_\parallel, z, \boldsymbol{T}) \chi_l(z). \tag{3.13}$$

Inserting (3.11), we find that this is a plain three-dimensional Fourier transform:

$$F_l(\boldsymbol{q}, \boldsymbol{T}) = \int \mathrm{d}^3 r \, \mathrm{e}^{i\boldsymbol{q}\boldsymbol{r}} F(\boldsymbol{r}, \boldsymbol{T}) \chi_l(z). \tag{3.14}$$

Except for the restriction to layer l, it is the standard form factor that appears in the regular (plane-wave) Born approximation. Therefore, it is occasionally called the *Born form factor*, and so we will call it. (3.12) and (3.13) remain applicable if the plane waves $\phi^\pm(z)$ are *damped* due to an imaginary part of the refractive index.

Currently, the summation over l in (3.12) is not implemented in BornAgain. Therefore particles must not extend beyond layer interfaces. This restriction will be lifted in one of the next releases.

To describe how (3.14) is evaluated in BornAgain, we need to specify some of the parameters contained in the generic parameter vector $\boldsymbol{T} \coloneqq (\Delta v_\mathrm{p}, Z, \boldsymbol{\Omega}, \boldsymbol{U})$: Δv_p is the SLD difference between the particle and the embedding matrix, as discussed in Sec. 3.1; for an inhomogeneous particle, it is some reference value obtained e. g. from the maximum SLD. Z is the vertical location of the particle; in our formalism, it is the vertical component of the position vector $\boldsymbol{R}$. $\boldsymbol{\Omega}$ is a tuple of rotation angles; they determine a rotation matrix $D_{\boldsymbol{\Omega}}$ that shall be defined by its action

$$F(\boldsymbol{r}, \Delta v_\mathrm{p}, Z, \boldsymbol{\Omega}, \boldsymbol{U}) = F(D_{\boldsymbol{\Omega}}^{-1} \boldsymbol{r}, \Delta v_\mathrm{p}, Z, \boldsymbol{0}, \boldsymbol{U}). \tag{3.15}$$

Finally, $\boldsymbol{U}$ collects all remaining parameters, among them size and shape parameters that determine the geometry and thereby the refractive index profile of the particle. With this, we can express the generic Born form factor as

$$F(\boldsymbol{q}, \Delta v_\mathrm{p}, Z, \boldsymbol{\Omega}, \boldsymbol{U}) = \Delta v_\mathrm{p} \mathrm{e}^{iq_\parallel Z} F(D_{\boldsymbol{\Omega}} \boldsymbol{q}, \boldsymbol{U}), \tag{3.16}$$

introducing the standard form factor

$$F(\boldsymbol{q}, \boldsymbol{U}) \coloneqq F(\boldsymbol{q}, 1, 0, \boldsymbol{0}, \boldsymbol{U}). \tag{3.17}$$

BornAgain comes with a comprehensive library of form factors, described in a dedicated Form Factor Catalog.

3.3 Decoupling approximations

In the DWBA matrix element (3.8), particle positions, orientations, shapes, and sizes can be coupled in arbitrary ways. To proceed any further, we need to specify this coupling at least in statistical terms. This can in principle be done in two different ways: Either through physical models, implemented within BornAgain, or by loading a representative set $\{\boldsymbol{R}_i, \boldsymbol{T}_i\}$ from an external *morphology* file that could be generated from simulations, or from electron microscopy images.

Import of *morphology data*, pioneered by `IsGISAXS` [2, Sec. 3.3], is not yet implemented in BornAgain, and not on our agenda. Please contact us if you have a use case.

BornAgain provides various physical models for the distribution of $\boldsymbol{R}_i$ and $\boldsymbol{T}_i$. Except if uniform particles form a perfect two-dimensional crystal, some degrees of freedom will be more or less disordered. Therefore the models need to be formulated in a statistical language. That formalism is then versatile enough to also cover any degree of order.

To prepare a statistical formulation, we encode the particle coordinates in a distribution function

$$\mathcal{P}(\boldsymbol{r}, \boldsymbol{\tau}, \boldsymbol{\tau}') := \sum_{jk} \delta^2(\boldsymbol{r} - (\boldsymbol{R}_{j\parallel} - \boldsymbol{R}_{k\parallel})) \delta^n(\boldsymbol{\tau} - \boldsymbol{T}_j) \delta^n(\boldsymbol{\tau}' - \boldsymbol{T}_k). \tag{3.18}$$

The exponents denote the dimensionalities of the delta-functions; n is the dimensionality of $\boldsymbol{\tau}$. Its total integral is

$$\int \mathrm{d}^2 r \int \mathrm{d}\boldsymbol{\tau} \, \mathrm{d}\boldsymbol{\tau}' \mathcal{P}(\boldsymbol{r}, \boldsymbol{\tau}, \boldsymbol{\tau}') = N_p^2, \tag{3.19}$$

where N_p is the number of particles, the integration over $\boldsymbol{r}$ is restricted to the horizontal plane, and the differential $\mathrm{d}\boldsymbol{\tau}$ is to be understood as $\mathrm{d}^n \tau$. In later approximations, (3.19) will be a normalization requirement. The differential cross section (3.9) can now be written as

$$\frac{\mathrm{d}\sigma}{\mathrm{d}\Omega} = \int \mathrm{d}^2 r \, \mathrm{e}^{i\boldsymbol{q}_\parallel \boldsymbol{r}} \int \mathrm{d}\boldsymbol{\tau} \, \mathrm{d}\boldsymbol{\tau}' \mathcal{P}(\boldsymbol{r}, \boldsymbol{\tau}, \boldsymbol{\tau}') \mathcal{F}(\boldsymbol{\tau}) \mathcal{F}^*(\boldsymbol{\tau}'), \tag{3.20}$$

In the following, we will present different physical models that provide computable approximations for the formally exact distribution (3.18).

For the time being, we only support models that make the following assumption about the particle *properties* like shape, size, and orientation (but *not* position) that are encoded in the vector $\boldsymbol{T}_j$:

T-T decoupling approximation: Properties of different particles are not correlated.

In other words, the $\boldsymbol{T}_j$ are independent and identically distributed (*i.i.d.*) random variables. They all have the same distribution $p(\boldsymbol{\tau})$. Averages under this distribution shall be denoted as

$$\langle f \rangle := \int \mathrm{d}\boldsymbol{\tau} \, p(\boldsymbol{\tau}) f(\tau). \tag{3.21}$$

Pairs of particles have the distribution $p(\boldsymbol{\tau}) p(\boldsymbol{\tau}')$, except if the two particles are identical. In consequence, the distribution $\mathcal{P}$ must have the form

$$\mathcal{P}(\boldsymbol{r}, \boldsymbol{\tau}, \boldsymbol{\tau}') = N_p \{ \delta(\boldsymbol{r}) p(\boldsymbol{\tau}) \delta(\boldsymbol{\tau} - \boldsymbol{\tau}') + \left[\mathcal{G}(\boldsymbol{r}|\boldsymbol{\tau}, \boldsymbol{\tau}') - \delta(\boldsymbol{r}) \right] p(\boldsymbol{\tau}) p(\boldsymbol{\tau}') \} \tag{3.22}$$

with the conditional position correlation function $\mathcal{G}$. Inserting this in (3.20) we obtain

$$\frac{1}{N_p} \frac{\mathrm{d}\sigma}{\mathrm{d}\Omega} = I_\mathrm{d} + I_\mathrm{c} \tag{3.23}$$

with the *diffuse* and *coherent* scattering intensities

$$I_{\rm d} \quad := \quad \langle |\mathcal{F}|^2 \rangle - |\langle \mathcal{F} \rangle|^2 \,, \tag{3.24}$$

$$I_{\rm c} \quad := \quad \int {\rm d}^2 r \, e^{i\boldsymbol{q}_\parallel \boldsymbol{r}} \int {\rm d}\boldsymbol{\tau} \, {\rm d}\boldsymbol{\tau}' \mathcal{G}(\boldsymbol{r}|\boldsymbol{\tau}, \boldsymbol{\tau}') p(\boldsymbol{\tau}) p(\boldsymbol{\tau}') \mathcal{F}(\boldsymbol{\tau}) \mathcal{F}^*(\boldsymbol{\tau}'). \tag{3.25}$$

The diffuse intensity can be rewritten as

$$I_{\rm d} = \langle |\mathcal{F} - \langle \mathcal{F} \rangle|^2 \rangle \,, \tag{3.26}$$

which shows that it is due to fluctuations of the single-particle form factor.

To proceed further, we need to make approximations for the distribution $\mathcal{G}$. Only a few paracrystal models actually specify a conditioning of $\mathcal{G}$ on the particle properties $\boldsymbol{\tau}, \boldsymbol{\tau}'$. For all other models, we assume the

R-T decoupling approximation: Particle positions do not depend on properties.

Hence simply $\mathcal{G}(\boldsymbol{r}|\boldsymbol{\tau}, \boldsymbol{\tau}') = \mathcal{G}(\boldsymbol{r})$. To distinguish $\mathcal{G}(\boldsymbol{r})$ from the standard *pair correlation function* at atomic level, we will call it the *particle position correlation function*. The Fourier transform

$$\mathcal{S}(\boldsymbol{q}) := \int {\rm d}^2 r \, e^{i\boldsymbol{q}_\parallel \boldsymbol{r}} \mathcal{G}(\boldsymbol{r}) \tag{3.27}$$

shall be called the *interference function*. It is the two-dimensional, mesoscale equivalent of the atomic *static structure factor* (in crystallography also called *lattice factor*). The coherent scattering intensity then takes the simple form

$$I_{\rm c} = \mathcal{S}(\boldsymbol{q}) \, |\langle \mathcal{F} \rangle|^2 \,. \tag{3.28}$$

Together, the T-T and R-T decoupling make up the *decoupling approximation* of `IsGISAXS`.[2] In BornAgain, R-T decoupling is the default. Only a few models explicitly introduce some size-position coupling. The following sections are therefore mostly concerned with models for $\mathcal{S}(\boldsymbol{q})$.

If a user-defined sample model leaves the interference function unspecified, then the default (`InterferenceFunctionNone`) is simply $\mathcal{S}(\boldsymbol{q}) = 1$, which is a valid model for *dilute* particles. $I_{\rm c}$ then cancels the second term in Sec. 3.3, so that the cross section (3.23) reduces to the incoherent sum

$$\frac{1}{N_p} \frac{{\rm d}\sigma}{{\rm d}\Omega} = \langle |\mathcal{F}|^2 \rangle \tag{3.29}$$

---

[2] In the `IsGISAXS` manual [2, Sec. 2.2], the *decoupling approximation* (DA) is opposed to the *local monodisperse approximation* (LMA) and the *size-spacing correlation approximation* (SSCA). We can now disentangle this skew trichotomy: The LMA is opposite to coherent superposition; it describes the incoherent sum of scattering from different coherence domains. In BornAgain, it can be emulated by averaging over different simulated GISAS images (as described in Sec. 1.3), or by attaching different `ParticleLayout`s to a `Layer`. The SSCA is an alternative to the R-T decoupling approximation. In `IsGISAXS`, and similarly in BornAgain, it is only available for paracrystals (Sec. 3.5).

3.4 Lateral order of nanoparticles

3.4.1 One-dimensional lattice

For a perfect one-dimensional lattice along the x-axis with period a, the position correlation function is given by:

$$\rho_S \mathcal{G}(\boldsymbol{r}) = \sum_{n \neq 0} \delta(x - na)\delta(y). \tag{3.30}$$

Using standard relations for the Dirac comb, one obtains the interference function

$$\mathcal{S}(\boldsymbol{q}) = \frac{2\pi}{a} \sum_k \delta\left(q_x - \frac{2\pi k}{a}\right), \tag{3.31}$$

which has the reciprocal lattice period $2\pi/a$.

For computational reasons in BornAgain, the delta functions appearing in the interference function are replaced by distributions of a finite width $H(q_x - 2\pi k/a)$. This amounts to convoluting the previously given interference function with $H(q_x)$ or, equivalently, multiplying the position correlation function by the inverse Fourier image of $H(q_x)$, called the *decay function* $h(x)$.

The interference function can then be written as:

$$\mathcal{S}(q_x) = \frac{1}{a} \sum_k H\left(q_x - \frac{2\pi k}{a}\right). \tag{3.32}$$

BornAgain currently supports the following types of one-dimensional decay functions (parameterized by a decay length λ):

Name	$h(x)$	$H(q_x)$
Cauchy	$\mathrm{e}^{-|x|/\lambda}$	$\frac{2\lambda}{1+q_x^2\lambda^2}$
Gauss	$\mathrm{e}^{-x^2/2\lambda^2}$	$\sqrt{2\pi}\lambda\mathrm{e}^{-q_x^2\lambda^2/2}$
Triangle	$1 - |x|/\lambda \quad \text{for} \quad |x| < \lambda$	$\lambda\,\mathrm{sinc}^2(q_x\lambda/2)$

$$(3.33)$$

In addition, a pseudo-Voigt decay function is available, which is a convex combination of the Cauchy and Gauss decay functions. The decay functions are all normalized such that $\int \mathrm{d}q_x H(q_x) = 2\pi$, which is equivalent to $h(0) = 1$. If the one-dimensional lattice is rotated with respect to the x-axis by an angle ξ, the corresponding interference function is calculated by using the correct projection of the in-plane reciprocal vector instead of q_x:

$$q_\xi = q_x \cos \xi + q_y \sin \xi. \tag{3.34}$$

3.4.2 Two-dimensional lattice

For a perfect two-dimensional lattice with lattice basis $(\boldsymbol{a}, \boldsymbol{b})$, the position correlation function is given by:

$$\rho_S \mathcal{G}(\boldsymbol{r}) = \sum_{m,n} \delta(\boldsymbol{r} - m\boldsymbol{a} - n\boldsymbol{b}) - \delta(\boldsymbol{r}). \qquad (3.35)$$

The corresponding interference function then becomes

$$\mathcal{S}(\boldsymbol{q}) = 4\pi^2 \rho_S \sum_{\boldsymbol{q}_i \in \Lambda^*} \delta(\boldsymbol{q} - \boldsymbol{q}_i), \qquad (3.36)$$

where Λ^* denotes the reciprocal lattice of $(\boldsymbol{a}, \boldsymbol{b})$.

In BornAgain, the two-dimensional delta functions need to be replaced again with distributions of finite width $H(\boldsymbol{q} - \boldsymbol{q}_i)$. Currently, BornAgain only allows for two-dimensional decay functions that are defined in the radial variable

$$\phi := \sqrt{X^2/\lambda_X^2 + Y^2/\lambda_Y^2}, \qquad (3.37)$$

where (X, Y) are the coordinates in an orthonormal coordinate system, where the X-axis is rotated by an angle γ with respect to the first lattice vector $\boldsymbol{a}$. This amounts to convoluting the previously given interference function with $H(\boldsymbol{q})$ or, equivalently, multiplying the position correlation function by the inverse Fourier image of $H(\boldsymbol{q})$, called the *decay function $h(\phi)$*.

The interference function can then be written as:

$$\mathcal{S}(\boldsymbol{q}) = \rho_S \sum_{\boldsymbol{q}_i \in \Lambda^*} H(\boldsymbol{q} - \boldsymbol{q}_i). \qquad (3.38)$$

BornAgain currently supports the following types of two-dimensional decay functions (parameterized by two decay lengths λ_X, λ_Y):

Name	$h(\phi)$	$H(Q)$
Cauchy	$\mathrm{e}^{-\phi}$	$\frac{2\pi\lambda_X\lambda_Y}{(1+Q^2)^{3/2}}$
Gauss	$\mathrm{e}^{-\phi^2/2}$	$2\pi\lambda_X\lambda_Y\mathrm{e}^{-Q^2/2}$

$$(3.39)$$

with $Q := \sqrt{q_X^2\lambda_X^2 + q_Y^2\lambda_Y^2}$.

In addition, a pseudo-Voigt decay function is available, which is a convex combination of the Cauchy and Gauss decay functions. The decay functions are all normalized such that $\int \mathrm{d}^2q_\parallel H(\boldsymbol{q}) = 4\pi^2$, which is equivalent to $h(0) = 1$.

3.5 Paracrystals

3.5.1 The one-dimensional paracrystal

A paracrystal, originally developed by Hosemann [22], models the cumulative disorder of the interparticle distances. Although the paracrystal in one dimension is not directly implemented in BornAgain, it forms the basis for the paracrystal models in BornAgain and will thus be discussed first.

In one dimension, the paracrystal is parameterized by the position distribution of the nearest neighbour $p(x)$, centered at a peak distance D. The probablility distribution of the position of the nearest neighbour to the right of the particle at the origin then becomes

$$p_1(x) = p(x - D). \tag{3.40}$$

The position distribution function for the next to nearest neighbour is then the convolution of this distribution with itself (probability of finding the nearest neighbour at x' times the probability of finding the next particle at distance $x - x'$ from the first and then integrate over x'):

$$p_2(x) = p(x - D) \otimes p(x - D). \tag{3.41}$$

The probability distribution of finding a particle to the right of the particle at the origin then becomes:

$$\rho_S \mathcal{G}^+(x) = \sum_{n>0} \otimes^n p(x - D). \tag{3.42}$$

The probability at the left side is just the mirror image: $\mathcal{G}^-(x) = \mathcal{G}^+(-x)$. After taking the Fourier transform, the interference function is

$$\mathcal{S}(q_x) = 1 + 2\operatorname{Re}\left(\frac{P(q_x)}{1 - P(q_x)}\right) = \operatorname{Re}\left(\frac{1 + P(q_x)}{1 - P(q_x)}\right), \tag{3.43}$$

where $P(q_x)$ is the Fourier transform of $p(x - D)$.

Since the Fourier transformed distribution $P(q_x)$ will always be 1 at $q_x = 0$, there is a singularity at the origin of $\mathcal{S}(q_x)$. This singularity is caused by the forward scattering contribution of an infinitely long lattice and can be removed in two ways in BornAgain. The simplest way is to multiply $P(q_x)$ by a fixed factor that is very close, but not equal to, one:

$$P'(q_x) \coloneqq P(q_x)\mathrm{e}^{-D/\Lambda}, \tag{3.44}$$

where Λ has dimension of length and is called the damping length.

A second possibility for removing the singularity at $q_x = 0$ consists of considering only a finite portion of the one-dimensional paracrystal. Caution has to be taken here, since the probability distributions at either side of the particle will depend on which

particle of the finite lattice is considered. The calculations can still be carried out exactly and lead to the following expression for the interference function:

$$\mathcal{S}(q_x) = 1 + 2\,\mathrm{Re}\left(\frac{P(q_x)}{1 - P(q_x)} - \frac{P(q_x)\left[1 - P^{N_p}(q_x)\right]}{N_p\left(1 - P(q_x)\right)^2}\right), \tag{3.45}$$

with N_p the number of particles making up the finite lattice.

Before embarking on the paracrystal models, implemented in BornAgain, it has to be stressed that there is no such thing as a paracrystal in more than one dimension. The following models are consequently only to be seen as ad hoc approximations of lattices with cumulative disorder.

3.5.2 The radial paracrystal

In the radial paracrystal model, the interference function of the one-dimensional para-crystal is used directly, but applied to the radial component of $\boldsymbol{q}_{\parallel}$. The resulting interference function, which is radially symmetric, is then given by

$$\mathcal{S}(\boldsymbol{q}_{\parallel}) = \mathrm{Re}\left(\frac{1 + P(q_{\parallel})}{1 - P(q_{\parallel})}\right), \tag{3.46}$$

or one of the versions with the singularity removed.

In BornAgain, the following one-dimensional distribution functions for $p(x)$ are implemented:

Name	$p(x)$	$P(q_x)$
Cauchy	$\frac{1}{2\omega}\exp(-|x|/\omega)$	$\frac{1}{1 + q_x^2\omega^2}$
Gauss	$\frac{1}{\omega\sqrt{2\pi}}\exp(-x^2/2\omega^2)$	$\exp(-q_x^2\omega^2/2)$
Gate	$\frac{1}{2\omega}$ for $|x| < \omega$	$\mathrm{sinc}(q_x\omega)$
Triangle	$\frac{1}{\omega}\left(1 - |x|/\omega\right)$ for $|x| < \omega$	$\mathrm{sinc}^2(q_x\omega/2)$
Cosine	$\frac{1}{2\omega}\left(1 + \cos(\pi x/\omega)\right)$ for $|x| < \omega$	$\frac{\mathrm{sinc}(q_x\omega)}{1 - (q_x\omega/\pi)^2}$

$$\tag{3.47}$$

In addition, a pseudo-Voigt distribution function is available, which is a convex combination of the Cauchy and Gauss distribution functions.

For the radial paracrystal, there is also an extension available in BornAgain that takes into account a coupling between the size of the particles and the inter-particle distance. This approximation is discussed in more detail in 3.5.4.

3.5.3 The two-dimensional paracrystal

The two-dimensional paracrystal model in BornAgain is implemented as a simple convolution of the two one-dimensional paracrystals along the lattice basis vectors. The calculation of the interference function results in a simple product of two one-dimensional interference functions:

$$\mathcal{S}(\boldsymbol{q}) = \mathrm{Re}\left(\frac{1 + P_1(\boldsymbol{q})}{1 - P_1(\boldsymbol{q})}\right)\mathrm{Re}\left(\frac{1 + P_2(\boldsymbol{q})}{1 - P_2(\boldsymbol{q})}\right), \tag{3.48}$$

where $P_1(\boldsymbol{q})$ and $P_2(\boldsymbol{q})$ denote the Fourier transforms of the two independent particle distributions (which are now both two-dimensional distribution functions).

Again, BornAgain provides for removing the singularity by either using a damping length or by indicating finite domain sizes.

The two-dimensional distributions supported in BornAgain are parameterized by

$$\phi := \sqrt{X^2/\omega_X^2 + Y^2/\omega_Y^2}, \tag{3.49}$$

where (X, Y) are the coordinates in an orthonormal coordinate system, where the X-axis is rotated by an angle γ with respect to the first lattice vector $\boldsymbol{a}$.

The following distributions are currently supported:

Name	$p(\phi)$	$P(Q)$
Cauchy	$\frac{1}{2\pi\omega_X\omega_Y}\exp(-\phi)$	$\frac{1}{(1+Q^2)^{3/2}}$
Gauss	$\frac{1}{2\pi\omega_X\omega_Y}\exp(-\phi^2/2)$	$\exp(-Q^2/2)$
Gate	$\frac{1}{\pi\omega_X\omega_Y}$ for $\phi < 1$	$\frac{2J_1(Q)}{Q}$
Cone	$\frac{3}{\pi\omega_X\omega_Y}(1-\phi)$ for $\phi < 1$	$6\left[\frac{J_1(Q)}{Q} - \frac{1}{Q^3}\int_0^Q \mathrm{d}u u^2 J_0(u)\right]$

(3.50)

with $Q := \sqrt{q_X^2\omega_X^2 + q_Y^2\omega_Y^2}$.

Again, a convex combination of the Cauchy and Gauss distributions in two dimensions is available (pseudo-Voigt).

3.5.4 The radial paracrystal with size-position coupling

Restricting the calculation to one layer, the differential cross section for a specific arrangement of particles of different type is:

$$\frac{\mathrm{d}\sigma}{\mathrm{d}\Omega} = \sum_{ij} e^{i\boldsymbol{q}_\parallel(\boldsymbol{R}_{j\parallel}-\boldsymbol{R}_{i\parallel})}\mathcal{F}(\boldsymbol{T}_i)\mathcal{F}^*(\boldsymbol{T}_j). \tag{3.51}$$

In a statistical ensemble, this cross section has to be averaged by the joint probability density function for all postions and types of each individual particle:

$$\mathcal{P}\left(\{\boldsymbol{R}_{i\parallel}\}, \{\boldsymbol{T}_i\}\right). \tag{3.52}$$

Its normalization is chosen such that the total integral over its phase space equals $N!$, with N the number of particles. This reflects the arbitrary nature of the indices i for each particle and will be removed when we consider a specific choice for the indices.

The expectation value of the differential cross section then becomes

$$\left\langle\frac{\mathrm{d}\sigma}{\mathrm{d}\Omega}\right\rangle = \frac{1}{N!}\int\prod_i d^2\boldsymbol{R}_{i\parallel}d\boldsymbol{T}_i\,\mathcal{P}\left(\{\boldsymbol{R}_{i\parallel}\}, \{\boldsymbol{T}_i\}\right)\sum_{jk} e^{i\boldsymbol{q}_\parallel(\boldsymbol{R}_{k\parallel}-\boldsymbol{R}_{j\parallel})}\mathcal{F}(\boldsymbol{T}_j)\mathcal{F}^*(\boldsymbol{T}_k). \tag{3.53}$$

As for the case of the radial paracrystal, a one-dimensional approach is developed, which is then applied to the radial component of the wavevector transfer. In this approach, we can replace the radial postion $\boldsymbol{R}_{i\parallel}$ with x_i.

For a one-dimensional arrangement of particles, we can choose the indices of the particles such that they increase with their position x_i. If the joint probability density function is adapted to only have support for particles ordered in this way, we can drop the factor $1/N!$ in the expectation value.

For each term appearing in the sum of the integrand of the expectation value of the cross section, we only need to know the density function of the positions and types of two particles, denoted by their indices j and k. All other dependencies should be integrated out. In [23], this approach is used to calculate the effects of different types of correlations between sizes and/or positions on the diffuse scattering intensity. In BornAgain only a specific case is implemented, namely the one also appearing in the IsGisaxs software package as the *size-spacing correlation approximation* [2].

In this case, the distribution of the inter-neighbor distance between two particles depends only on the sizes of these two particles. Furthermore, the dependence is fixed to be a linear relationship of the mean distance d_n between particle $n-1$ and n and the particles' sizes ($X(\boldsymbol{T}_{n-1})$ and $X(\boldsymbol{T}_n)$):

$$\langle d_n \rangle = D + \kappa \left[\Delta X(\boldsymbol{T}_{n-1}) + \Delta X(\boldsymbol{T}_n) \right], \tag{3.54}$$

where D is the average interparticle distance, κ is the coupling parameter determining how much this interparticle distance is influenced by the particles' sizes, and

$$\Delta X(\boldsymbol{T}_n) \coloneqq X(\boldsymbol{T}_n) - \langle X \rangle$$

is the deviation from the mean of the size of a particle of type $\boldsymbol{T}_n$.

The differential cross section (3.53) in this case can then be expressed as:

$$\frac{1}{N} \left\langle \frac{\mathrm{d}\sigma}{\mathrm{d}\Omega} \right\rangle = \int d\boldsymbol{T} \, \mathcal{P}(\boldsymbol{T}) \, |\mathcal{F}(\boldsymbol{q}, \boldsymbol{T})|^2 + 2 \operatorname{Re} \left\{ \mathcal{F}_\kappa(\boldsymbol{q}) \tilde{\mathcal{F}}_\kappa(\boldsymbol{q}) \cdot \frac{P(q_\parallel)}{1 - \tilde{p}_{2\kappa}(q_\parallel) P(q_\parallel))} \right\}, \tag{3.55}$$

with

$$\tilde{p}_\kappa(q_\parallel) \coloneqq \int d\boldsymbol{T} \, \mathcal{P}(\boldsymbol{T}) e^{i\kappa q_\parallel \Delta X(\boldsymbol{T})},$$

$$\mathcal{F}_\kappa(\boldsymbol{q}) \coloneqq \int d\boldsymbol{T} \, \mathcal{P}(\boldsymbol{T}) e^{i\kappa q_\parallel \Delta X(\boldsymbol{T})} \mathcal{F}(\boldsymbol{q}, \boldsymbol{T}),$$

$$\tilde{\mathcal{F}}_\kappa(\boldsymbol{q}) \coloneqq \int d\boldsymbol{T} \, \mathcal{P}(\boldsymbol{T}) e^{i\kappa q_\parallel \Delta X(\boldsymbol{T})} \mathcal{F}^*(\boldsymbol{q}, \boldsymbol{T})$$

and $P(q_\parallel)$ is the Fourier transform of the average next neighbor distance (as was also the case for the radial paracrystal).

3.6 Disordered assemblies

... to be written ...

4 Instrument simulation

4.1 Incoming beam and resolution

… to be written …

4.2 Detector images

To conclude this chapter on the foundations of small-angle scattering, we shall derive the geometric factors that allow us to convert differential cross sections into detector counts. We shall also discuss how to present data on a physically meaningful scale.

4.2.1 Pixel coordinates, scattering angles, and q components

We assume that scattered radiation is detected in a flat, two-dimensional detector that generates histograms on a rectangular grid, consisting of $n \cdot m$ pixels of constant width and height, as sketched in Fig. 4.1. This figure also shows the coordinate system according to unanimous GISAS convention, with z normal to the sample plane, and with the incident beam in the xz plane. The origin is at the center of the sample surface. We suppose that the detector is mounted perpendicular to the x axis at a distance L from the sample position. The real-space coordinate at the center of pixel (i, j) is (L, y_i, z_i). Each pixel has a width Δy and a height Δz. BornAgain requires a full parametrization of the detector geometry to correctly perform the affine-linear mapping from pixel indices i, j to pixel coordinates x_i, y_i; see the rectangular detector tutorial.

Since the differential scattering cross section (1.48) is given with respect to a solid-angle element $d\Omega$, we need to express the scattered wavevector $\boldsymbol{k}_{\mathrm{f}}$ in spherical coordinates, using the horizontal azimuth angle ϕ_{f} and the vertical glancing angle α_{f}. The projection of $(\alpha_{\mathrm{f}}, \phi_{\mathrm{f}})$ into the detector plane (y, z) is known as the *gnomonic projection*. From elementary trigonometry one finds

$$
\begin{aligned}
y &= L \tan \phi_{\mathrm{f}}, \\
z &= (L / \cos \phi_{\mathrm{f}}) \tan \alpha_{\mathrm{f}}.
\end{aligned}
\tag{4.1}
$$

Fig. 4.2 shows lines of equal α_{f}, ϕ_{f} in the detector plane. To emphasize the curvature of the constant-α_{f} lines, scattering angles up to more than 25° are shown. In typical SAS or GISAS, scattering angles are much smaller, and therefore the mapping between
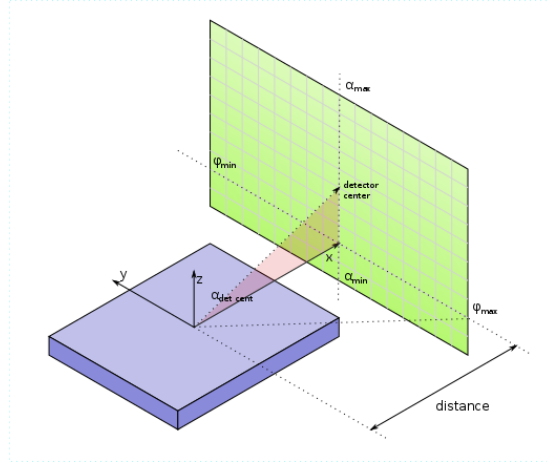
Figure 4.1: Experimental geometry with a two-dimensional pixel detector.

pixel coordinates and scattering angles is in a good first approximation linear. Of course BornAgain is not restricted to this linear regime, but uses the exact nonlinear mapping (4.1).

To determine the scattering vector $\boldsymbol{q}_{ij}$ that corresponds to a pixel (i, j), we need to express the outgoing wavevector $\boldsymbol{k}_{\mathrm{f}}$ as function of y and z. This can be done either by inverting (4.1) and inserting the so obtained $\alpha_{\mathrm{f}}(y, z)$ and $\phi_{\mathrm{f}}(y)$ in

$$
\boldsymbol{k}_{\mathrm{f}} = K \begin{pmatrix} \cos \alpha_{\mathrm{f}} \cos \phi_{\mathrm{f}} \\ \cos \alpha_{\mathrm{f}} \sin \phi_{\mathrm{f}} \\ \sin \alpha_{\mathrm{f}} \end{pmatrix},
\tag{4.2}
$$

or much more directly by using geometric similarity in Cartesian coordinates. The result is rather simple:

$$
\boldsymbol{k}_{\mathrm{f}} = \frac{K}{\sqrt{L^2 + y^2 + z^2}} \begin{pmatrix} L \\ y \\ z \end{pmatrix}.
\tag{4.3}
$$

The transform (4.6) between pixel coordinates y, z and physical scattering vector components q_y, q_z is nonlinear, due to the square-root term in the denominator of (4.3). For $y, z \ll L$, however, nonlinear terms loose importance.

The left detector frame in Fig. 4.3 shows circles of constant values of $\pm q_x$. For given steps in q_x, the distance between adjacent circles increases towards the detector center. From (1.60) and (4.3), one finds asymptotically for $y, z \to L$ that q_x goes with the square of the two other components of the scattering vector,

$$
\frac{q_x}{K} \doteq \frac{y^2 + z^2}{2L^2} \doteq \frac{q_y^2 + q_z^2}{2K^2}.
\tag{4.4}
$$
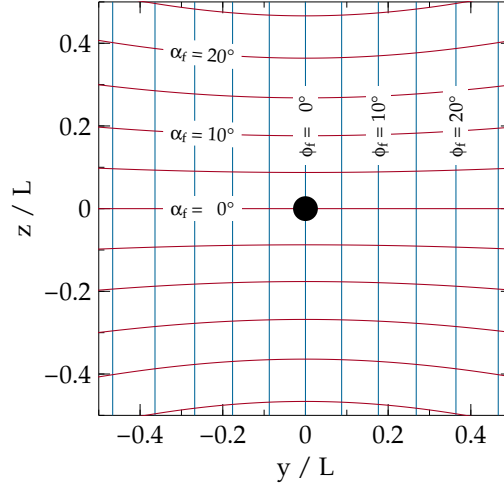
Figure 4.2: Lines of constant α_f (red) or ϕ_f (blue) in the detector plane, for a planar detector at distance L from the sample. The black dot indicates the beamstop location for the central incident beam (SAS geometry, $\hat{\boldsymbol{k}}_i = \hat{x}$).

Therefore, under typical small angle conditions $y, z \to L$ the dependence of the scattering signal on q_x is unimportant: one basically measures $v(\boldsymbol{q}) \simeq v(0, q_y, q_z)$. The exception, for sample structures with long correlations in x direction, is illustrated in Fig. 4.4.

As anticipated in (4.4), the other two components of $\boldsymbol{q}$ are in first order linear in the pixel coordinates,

$$\frac{q_y}{K} = \frac{y}{L}\left(1 - \frac{y^2 + z^2}{2L^2} + \dots\right), \tag{4.5}$$

and similarly for q_z. The nonlinear correction terms lead to the pincushion distortion shown in the right detector frame in Fig. 4.3.

Since pixel coordinates are meaningful only with respect to a specific experimental setup, users may wish to transform detector images towards the physical coordinates q_y and q_z. As shown in Fig. 4.5, this would yield a barrel-shaped illuminated area in the q_y, q_z plane.

To summarize this section, the wavevector $\boldsymbol{q}_{ij}$ can be determined from the pixel indices through the following steps:

$$(i, j)$$
$$\downarrow \quad \text{calibrate of origin, then employ affine-linear mapping}$$
$$(y, z)$$
$$\downarrow \quad \text{use (4.3)} \tag{4.6}$$
$$\boldsymbol{k}_f$$
$$\downarrow \quad \text{use (1.60)}$$
$$\boldsymbol{q}$$
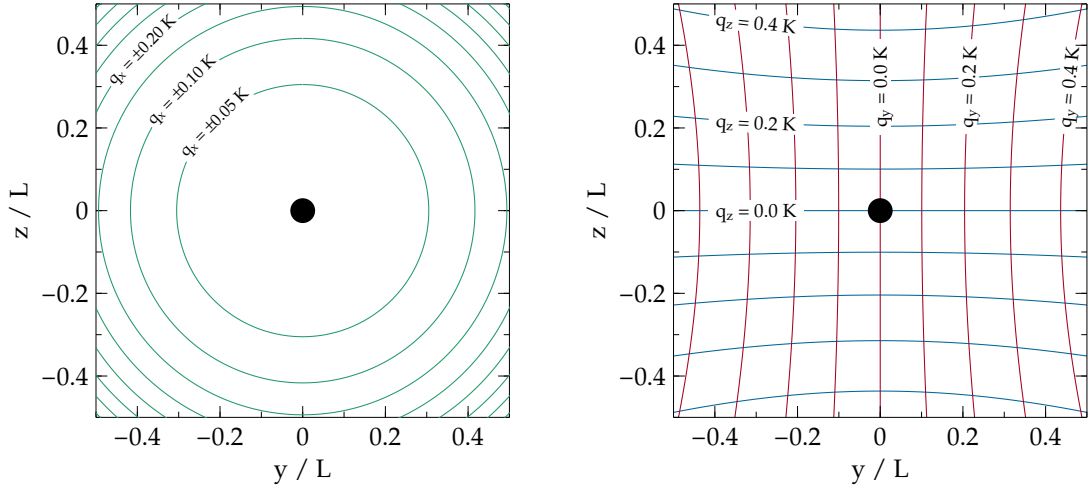
Figure 4.3: Lines of constant q_x (left), q_y or q_z (right), in units of the incident wavenumber $K = 2\pi/\lambda$, for a planar detector. SAS geometry as in Fig. 4.2.

Transforming detector images from pixel coordinates into the q_y, q_z plane is not implemented in BornAgain, and not on our agenda. We would, however, like to hear about use cases.

When simulating and fitting experimental data with BornAgain, detector images remain unchanged. All work is done in terms of reduced pixel coordinates y/L and z/L. Corrections are applied to the simulated, not to the measured data.

…show how to plot q grid on top of detector image …

4.2.2 Intensity transformation

The solid angle under which a detector pixel is illuminated from the sample is in linear approximation

$$\Delta\Omega = \cos\alpha_\mathrm{f}\,\Delta\alpha_\mathrm{f}\,\Delta\phi_\mathrm{f} = \cos\alpha_\mathrm{f}\left|\frac{\partial(\alpha_\mathrm{f},\phi_\mathrm{f})}{\partial(y,z)}\right|\Delta y\,\Delta z = \cos^3\alpha_\mathrm{f}\,\cos^3\phi_\mathrm{f}\,\frac{\Delta y\,\Delta z}{L^2}. \qquad (4.7)$$

Altogether, the expected count rate in detector pixel (i,j) is proportional to

$$I_{ij} = \cos^3\alpha_\mathrm{f}\,\cos^3\phi_\mathrm{f}\,\frac{\mathrm{d}\sigma}{\mathrm{d}\Omega}(\boldsymbol{q}_{ij}), \qquad (4.8)$$

where we have omitted constant factors L^{-2}, Δy and Δz. Using pixel coordinates instead of angles, this can be rewritten as

$$I_{ij} = \left(1 + \frac{y^2 + z^2}{L^2}\right)^{-3/2}\frac{\mathrm{d}\sigma}{\mathrm{d}\Omega}\big(\boldsymbol{q}_{ij}(y,z)\big). \qquad (4.9)$$
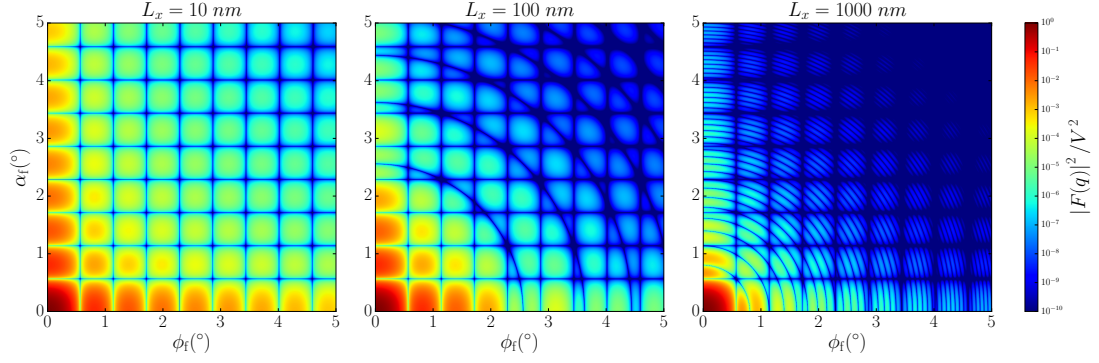
Figure 4.4: Simulated detector image for small-angle scattering from uncorrelated cuboids (right rectangular prisms). The incoming wavelength is 0.1 nm. The prisms have edge lengths $L_y = L_z = 10$ nm; the length L_x, in beam direction, is varied as shown above the plots. The circular modulation comes from a factor $\mathrm{sinc}(q_x L_x/2)$ in the cuboid form factor, with q_x given by (4.4).
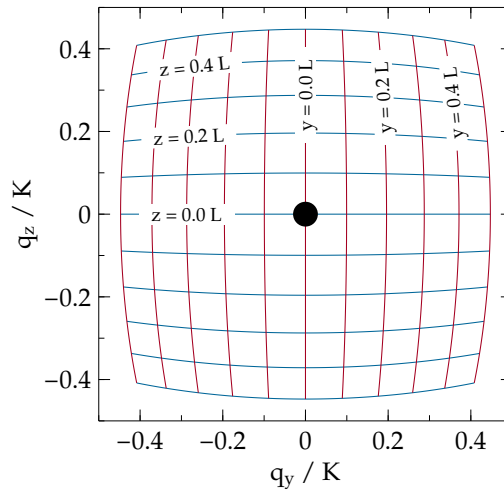
Figure 4.5: The outer contour of the blue and red grid shows the border of a square detector image after transformation into the physical coordinates q_y, q_z. The blue and red curves correspond to horizontal and vertical lines in the detector.

Bibliography

[1] G. Pospelov, W. Van Herck, J. Burle, J. M. Carmona Loaiza, C. Durniak, J. M. Fisher, M. Ganeva, D. Yurov and J. Wuttke, J. Appl. Cryst. **53**, 262 (2020). 5, 6, 7, 8

[2] R. Lazzari, *IsGISAXS*. Version 2.6. http://www.insp.jussieu.fr/oxydes/IsGISAXS/isgisaxs.htm (2006). 6, 33, 34, 40

[3] R. Lazzari, J. Appl. Cryst. **35**, 406 (2002). 6

[4] G. Renaud, R. Lazzari and F. Leroy, Surf. Sci. Rep. **64**, 255 (2009). 6, 9

[5] V. P. Sears, Neutron News **3**, 26 (1992). 8

[6] V. P. Sears, *Neutron Optics*, Oxford University Press: Oxford (1989). 8

[7] F. Mezei, Physica B+C **137**, 295 (1986). 8

[8] C. F. Majkrzak, K. V. O'Donovan and N. F. Berk, in *Neutron Scattering from Magnetic Materials*, edited by T. Chatterji, Elsevier: Amsterdam (2006). 8

[9] M. v. Laue, Erg. exakt Naturwiss. **10**, 133 (1931). 9

[10] H. Schober, J. Neutron Res. **17**, 109 (2014). 11

[11] G. H. Vineyard, Phys. Rev. B **26**, 4146 (1982). 11

[12] P. Mazur and D. L. Mills, Phys. Rev. B **26**, 5175 (1982). 11

[13] S. Dietrich and H. Wagner, Z. Phys. B **56**, 207 (1984). 11, 15

[14] S. Dietrich and H. Wagner, Z. Phys. B **59**, 35 (1985). 11, 15

[15] R. J. Potton, Rep. Progr. Phys. **67**, 717 (2004). 14

[16] S. Dietrich and H. Wagner, *Private communication* (2016). 15

[17] V. O. de Haan, J. Plomp, M. T. Rekveldt, A. A. van Well, R. M. Dalgliesh, S. Langridge, A. J. Böttger and R. Hendrikx, Phys. Rev. B **81**, 094112 (2010). 16

[18] C. F. Majkrzak, C. Metting, B. B. Maranville, J. A. Dura, S. Satja, T. Udovic and N. F. Berk, Phys. Rev. A **89**, 033851 (2014). 16

[19] F. Abelès, J. Phys. Radium **11**, 307 (1950). 25

[20] L. G. Parratt, Phys. Rev. **95**, 359 (1954). 25

[21] J. D. Jackson, *Classical Electrodynamics*, John Wiley: New York (^{2}1975). 28

[22] R. Hosemann, Acta Cryst. **4**, 520 (1951). 37

[23] F. Leroy, R. Lazzari and G. Renaud, Acta Cryst. A **60**, 565 (2004). 40

List of Symbols

$\perp$ Normal to the xy sample plane, 24

$\parallel$ Parallel to the xy sample plane, 24

$\pm$ Upward $(+)$ or downward $(-)$ propagating, 25

α Polarization state index, 15

α_{f} Glancing angle of the detected beam, 24

α_{i} Glancing angle of the incident beam, 24

β Imaginary part of the refractive index, 13

$\delta v_l(\boldsymbol{q})$ Fourier transform of the SLD $\delta v(\boldsymbol{r})$, evaluated in one sample layer, 28

δ Small parameter in the refractive index $n = 1 - \delta + i\beta$, 13

$\delta\epsilon(\boldsymbol{r})$ Part of the permittivity $\epsilon(\boldsymbol{r})$ that causes scattering, 19

ϵ_0 Vacuum permittivity, 8.854...As/Vm, 10

$\epsilon(\boldsymbol{r})$ Relative dielectric permittivity function, 11

$\bar{\epsilon}(\boldsymbol{r})$ Part of the permittivity $\epsilon(\boldsymbol{r})$ that can be analytically handled, 19

$\boldsymbol{\epsilon}(\boldsymbol{r})$ Relative dielectric permittivity tensor, 10

$\boldsymbol{\Lambda}(\boldsymbol{r})$ Distortion field, 13

μ_0 Vacuum permeability, $4\pi \cdot 10^{-7}$ Vs/Am, 10

μ_{n} Magnetic moment of the neutron, 10

$\boldsymbol{\mu}(\boldsymbol{r})$ Relative magnetic permeability tensor, 10

$\hat{\rho}$ Density matrix operator, 9

$\rho(\boldsymbol{r})$ Electron number density, 11

ρ_s Number density of chemical element s, 9

σ Scattering or absorption cross section, 17

f	Subscript "final", 20
$G(r, r')$	Generic (possibly tensorial) Green function, 14
$G^\infty(r, r')$	Far-field approximation to the Green function $G(r, r')$, 15
$b(r)$	Rescaled field $b = (m\mu/2\pi\hbar^2)B$, 10
$B(r, t)$	Magnetic induction, 10
i	Subscript "incident", 14
$J(r)$	Flux, 9
$k_\perp$	Component of k along the sample normal, 24
k_l	Wavenumber in layer l, 26
k	Wave vector, 9
$k_\parallel$	Projection of k onto the sample plane, 24
K	Wavenumber in vacuum, 8
l	Layer index, 26
n_l	Refractive index of layer l, 26
n	Refractive index, 13
n	Normal vector of an interface, 32
N	A multilayer sample has N layers, including the semi-infinite bottom and top layers, 26
N_p	Number of scattering centers, 37
p_j	Probability of state j, 9
q	Scattering vector, 21
r_e	Classical electron radius $2.817\ldots^{-15}$ m, 11
r	Position, 8
s	Subscript "scattered", 15
S	Poyinting vector, 11
t	Time, 8
$\hat{u}$	Polarized field amplitude unit vector, 15
$U(r)$	Perturbation potential, 13

Index